



## Research Article

# Structure and properties of paleosols of the last two interglacial cycles of the Khovaling Loess Plateau, Tajikistan (Obi–Mazar section)

Olga A. Tokareva<sup>a,b,g</sup> , Marina P. Lebedeva<sup>c</sup>, Peter M. Sosin<sup>d</sup>, Islomov K. Ashurmadov<sup>e</sup>, Farhad Khormali<sup>g</sup> and Redzhep N. Kurbanov<sup>a,b,f</sup> 

<sup>a</sup>Institute of Geography RAS, Moscow, Russia; <sup>b</sup>Institute of Archeology and Ethnography SB RAS, Novosibirsk, Russia; <sup>c</sup>V.V. Dokuchaev Soil Science Institute RAS, Moscow, Russia; <sup>d</sup>Institute of Water Problems, Hydropower and Ecology NAST, Dushanbe, Tajikistan; <sup>e</sup>Institute of History, Archeology and Ethnography of NAST, Dushanbe, Tajikistan; <sup>f</sup>Faculty of Geography, Lomonosov Moscow State University, Moscow, Russia and <sup>g</sup>Gorgan University of Agricultural Sciences and Natural Resources, Iran

### Abstract

Significant thicknesses, a large number of paleosols, and an impressive chronological framework place the loess–paleosol series of the Afghan–Tajik depression on a par with the famous sections of the Chinese Loess Plateau. Based on the results of field stratigraphy, description of the macro- and micromorphological structure, field magnetic susceptibility measurements, and study of the chemical and grain-size compositions, a comprehensive characterization of the structure, properties, and formation conditions of paleosol horizons and loess layers was carried out. Three loess units and two pedocomplexes are distinguished in the late and upper middle Pleistocene deposits of the Obi–Mazar section. These sediments are characterized by high silt and carbonate content and the presence of loess with pedogenic features. Pedocomplex PC1, consisting of three paleosols, according to the stratigraphic position and absolute dating, corresponds to MIS 5. Pedocomplex PC2, consisting of two developed paleosols separated by loess, is correlated with MIS 7. The properties of the studied paleosols together with modern soil distribution in the region allow for the reconstruction of the soil type of PC1 and PC2 of the Obi–Mazar section with the genesis of the Calcisols–Kastanozems groups.

**Keywords:** Late and upper middle Pleistocene, Afgan–Tajik depression, calcareous soils, micromorphology, grain-size analysis

### Introduction

Research on the loess–paleosol series (LPS) of the Afghan–Tajik depression, initiated in the 1970s, focused on regional stratigraphy development (Lazarenko et al., 1977). Significant discovery of stone artifacts during geological studies was spearheaded by Ranov (Ranov, 1995; Ranov and Schäfer, 2000), which spurred extensive archaeological research. Among Tajik LPS, the Obi–Mazar section is notably rich in artifacts (Schäfer et al., 1996; Schäfer and Sosin, 2013). Research expanded to include stratigraphy, age, and properties of LPS sections (Lomov et al., 1982; Bronger et al., 1993, 1998a, b; Dodonov and Baiguzina, 1995; Dodonov, 2002), leading to a stratigraphic scheme based on thermoluminescence dating (Dodonov and Pen'kov, 1977; Schäfer et al., 1996), which was correlated with the oxygen isotope curve (Shackleton et al., 1995) and Chinese Loess Plateau sections (Ding et al., 2002). The Darai–Kalon section is now the most thoroughly studied geologically and paleopedologically (Frechen and Boergnik, 1997; Frechen and Dodonov, 1998; Dodonov et al., 1999).

Loesses in this region are aeolian, sourced from the Karakum and Kyzylkum deserts (Yang et al., 2006), and were deposited even during warm Pleistocene stages (Ranov and Schäfer, 2000; Dodonov, 2002). The Quaternary paleoclimate of southern Tajikistan was largely influenced by global orbital-scale climate patterns (Parviz et al., 2020). The stage of loess formation corresponding to the glacial stage in the piedmont took place in an arid and sharply continental climate (Dodonov et al., 1999).

Paleosols from the middle to late Pleistocene indicate warm, humid intervals (Dodonov and Baiguzina, 1995), forming complex, vertically extended profiles due to rapid loess accumulation (Lomov et al., 1982). Challenges arise in horizon identification and paleosol classification due to their polygenetic nature (Lomov, 1980; Bronger et al., 1995; Dodonov et al., 1999). Modern classifications are based primarily on Holocene soils with known soil-forming processes. Some researchers therefore describe soil genesis based on climatic stages rather than genetic horizons. Soil formation during the interglacial occurred in three climatic phases: “initial”, which was during the transition from glacial to interglacial with desert–steppe landscapes; “optimal”, which was during the wettest and warmest period with development of forest vegetation; and “final”, which was during gradual aridization with steppe and desert–steppe landscapes (Lomov and Sosin, 1976; Veklich, 1979; Lomov, 1980). The precipitation amount in the “optimal” phase was close to the current level (Pakhomov, 1991).

**Corresponding author:** Olga A. Tokareva; Email: [gidroliss@gmail.com](mailto:gidroliss@gmail.com).

**Cite this article:** Tokareva OA, Lebedeva MP, Sosin PM, Ashurmadov IK, Khormali F, Kurbanov RN (2025). Structure and properties of paleosols of the last two interglacial cycles of the Khovaling Loess Plateau, Tajikistan (Obi–Mazar section). *Quaternary Research* 1–17. <https://doi.org/10.1017/qua.2024.32>



The study of LPS and their implications for paleoenvironmental reconstruction in Tajikistan gained attention in the late twentieth century (Bronger *et al.*, 1993; Lomov *et al.*, 1996; Mestdagh *et al.*, 1999; Bronger and Smolíková, 2019). These and earlier investigations offered only a broad overview of the climatic signals found in the complete LPS of South Tajikistan (Lomov and Sosin, 1976; Lomov *et al.*, 1982; Schäfer *et al.*, 1998). The present study aims to identify soil-formation processes during the last two interglacial periods, associated with the first and second pedocomplexes (PC) and oxygen isotope stages 5 and 7, respectively (Frechen and Dodonov, 1998), focusing on microfeatures and chemical compositions of paleosols. This research provides insights into Pleistocene human settlement conditions in Central Asia, with cultural horizons typically associated with buried soils (Ranov, 1995; Khudzhageldiev, 2007; Kurbanov *et al.*, 2022).

### Study area

The Khovaling Loess Plateau, located in the northern Afghan-Tajik depression between the Hindu Kush, Pamir, and Gissar-Alai mountain systems (Fig. 1A), features extensive loess cover with thicknesses reaching 150–200 m, distributed across piedmonts and river terraces at altitudes of 300–2500 m (Dodonov and Pen'kov, 1977; Lomov and Ranov, 1985; Dodonov, 2002). The region's paleoclimate alternated between

warm, humid interglacials and dry, cold glacials. Currently, Obi-Mazar experiences average annual temperatures of 11–13°C and precipitation of 800–1000 mm (Mestdagh *et al.*, 1999; Yang and Ding, 2006), with 70% occurring from January to May, peaking in March and April (Häggi *et al.*, 2019). This climate supports a xeric soil-moisture regime (Soil Survey Staff, 2022) or dry subtropical conditions (Gerasimov and Glazovskaya, 1960). The Plateau is located in the northern subzone of the subtropical zone in the middle of Eurasia and the temperature is constantly mesic. The ratio of evaporation to precipitation is 1:3 (Scientific and Applied Handbook on the Climate of the USSR, 1988). Dust storms are frequent during the dry summer, driven by westerly winds carrying aeolian dust from Central Asian deserts, settling upon reaching the Pamir Plateau (Dodonov and Baiguzina, 1995).

Natural vegetation near the Obi-Mazar section includes mixed open conifer and broad-leaf forests with open meadows, which are often utilized for farming and grazing. Vegetation includes broad-leaf genera such as *Crataegus*, *Ziziphus*, *Acer*, *Ulmus*, *Populus*, and *Rosa*, and the coniferous *Juniperus*. Herbaceous genera found in this region are *Agropyron*, *Achillea*, *Malva*, *Hypericum*, *Melilotus*, *Origanum*, *Salvia*, *Cousinia*, *Prangos*, and *Ferula* (Dodonov *et al.*, 2006; Häggi *et al.*, 2019).

The region's soil types, ordered by increasing precipitation levels, are Regosols, Cambisols, Calcisols, and Kastanozems, as per

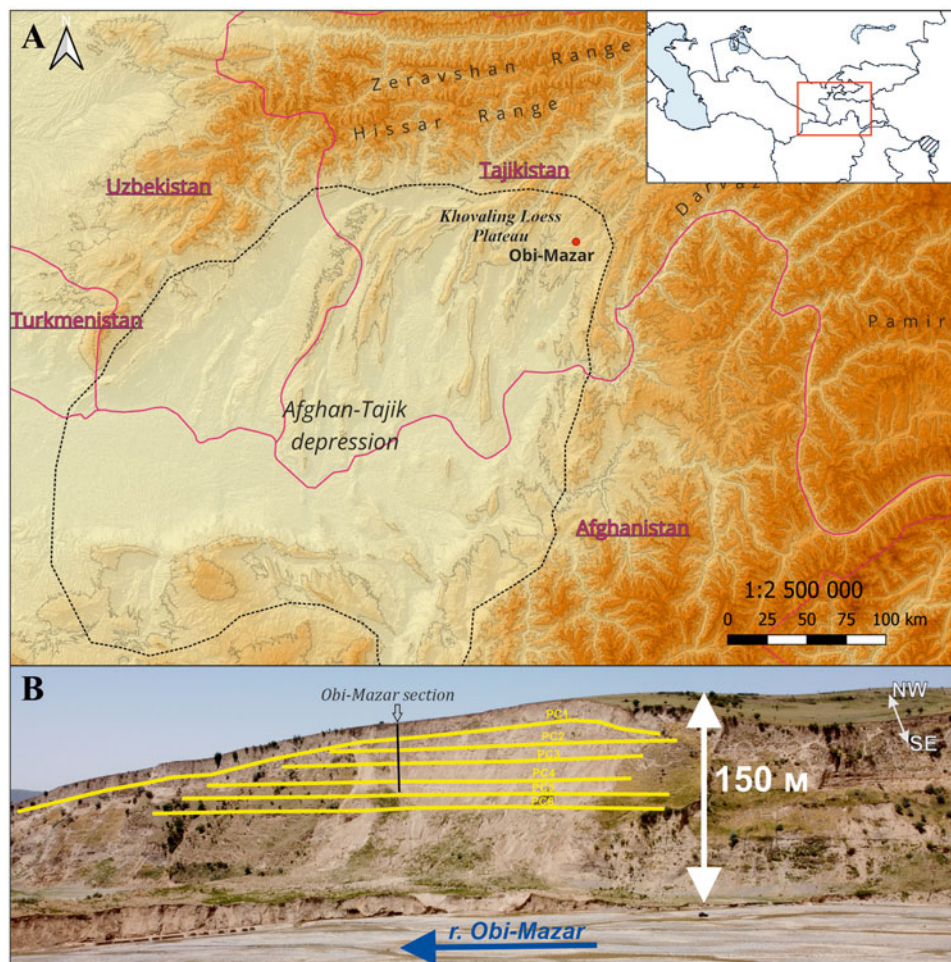


**Figure 1.** (A) Study area in the Afghan-Tajik depression. The red dot shows the location of the Obi-Mazar section. (B) General view of the outcrop and section of the Obi-Mazar. Yellow lines show the levels of occurrence of six identified pedocomplexes (PC); blue arrow shows flow direction of the Obi-Mazar River.



the World Reference Base for Soil Resources (IUSS Working Group WRB, 2022). Kastanozems, found under natural vegetation or minimally disturbed areas, degrade to Cambisols and Regosols on overgrazed or intensively plowed slopes (Dodonov et al., 2006; Khormali et al., 2024).

### Study section

The Obi-Mazar section (38°17'52.1"N, 69°53'01.6"E; 1300 m asl) is situated opposite the village of Lakhuti on the northwestern bank of the Obi-Mazar River in the Khovaling region of southern Tajikistan. The bank features a 150-meter-high outcrop composed of subaerial deposits approximately 80 meters thick, underlain by pebbly, sandy, and clayey alluvium (Fig. 1B). The LPS in the Obi-Mazar section comprises six pedocomplexes (Schäfer et al., 1998; Dodonov, 2002). The loess units were deposited under cold and arid conditions (glacials), while the paleosols developed during warm and humid periods (interglacials) (Bronger et al., 1995; Dodonov and Baiguzina, 1995). Our study focused on the upper 35 meters of the section, examining PC1, PC2, and the loess units separating them. Thermoluminescence (TL) dating

suggests that PC1 of the Khovaling Loess Plateau dates to approximately 71–127 ka, and PC2 dates to approximately 186–242 ka (Frechen and Dodonov, 1998).

### Methods

The Obi-Mazar section extends 35 m from the current surface, featuring a steep cliff (Fig. 2B), which complicates the study of its most complete and uneroded LPS at the center. To address this, three trenches were established: the uppermost for the Holocene section, the middle for maximum coverage of loess 1 (L1), and the lowest for examining paleosols PC1 and PC2.

Fieldwork involved preparing vertical walls in each trench, subdividing them into small sections or “pickets,” numbered top to bottom. Heights between adjacent pickets were measured using a water level, ensuring the trenches were positioned on stable loess and paleosols that were unaffected by landslides. Detailed lithological descriptions and macro-morphological characteristics of the deposits were recorded in the trenches. The horizon indices are given according to IUSS Working Group WRB (2022).

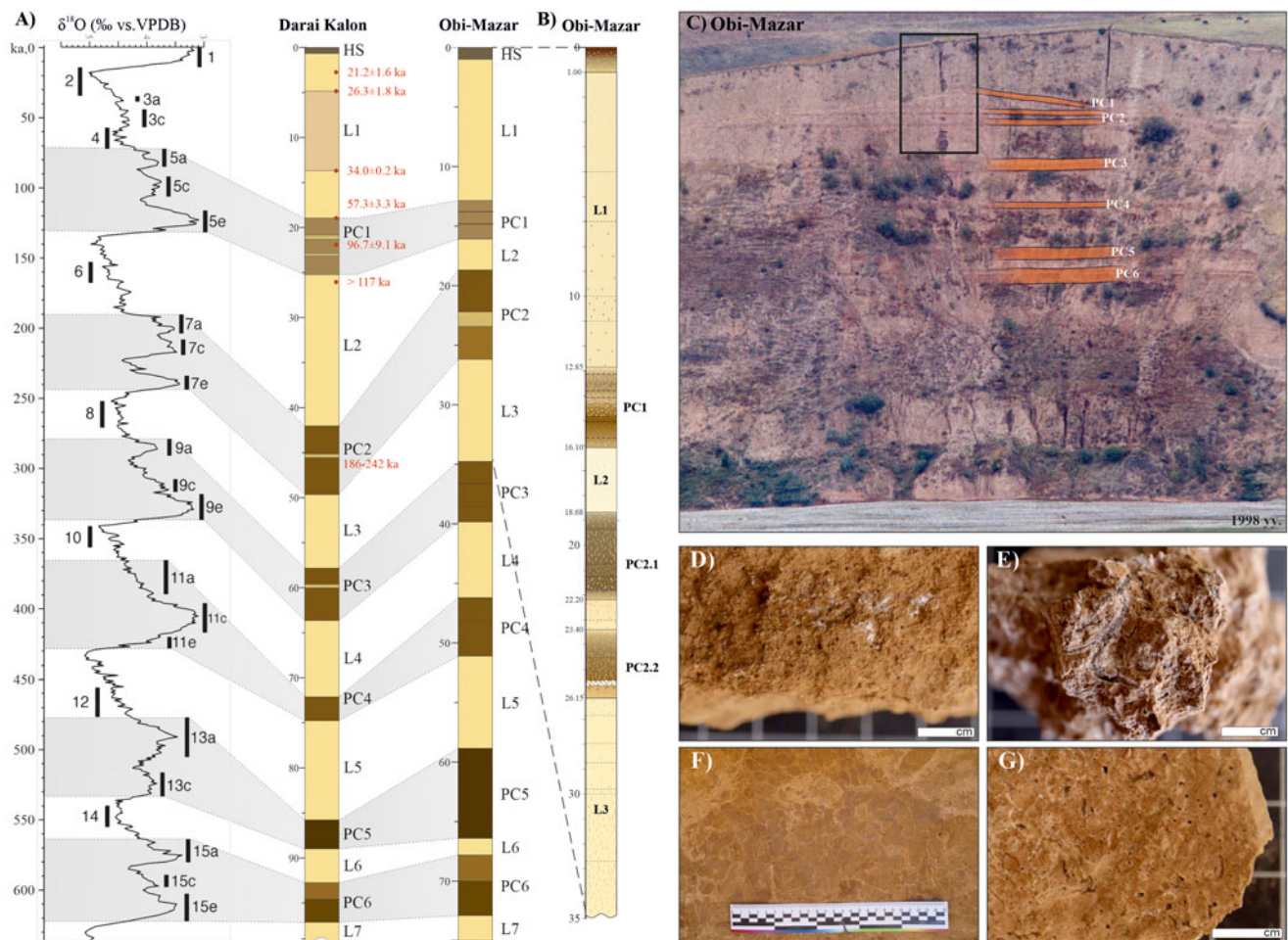


**Figure 2.** (A) Correlation of stratigraphic schemes of the Darai Kalon (modified after Dodonov et al., 2006) and Obi-Mazar sections with an optimized scheme of lettered marine isotope substages (Railsback et al., 2015a, b). Thermoluminescence dating of the Darai Kalon section was carried out by Frechen and Dodonov, 1998. VPDB = Vienna Pee Dee Belemnite; vertical scale in meters; gray-shaded bands show correlation intervals of the MIS scale with stratigraphic units; (B) stratigraphic scheme of the upper part of the Obi-Mazar section discussed in this paper. (C) General view of the Obi-Mazar outcrop (based on materials from Schäfer and Sosin, 2013); orange stripes indicate pedocomplexes; black rectangle indicates studied part of the loess–paleosol series deposits. (D–G) Macrophotographs of soil features: (D) calcite pseudomycelia, L1; (E) calcite pseudomycelia and organic-mineral coatings along the root channels, 2ABwk, PC1; (F) buried biolith capsules of invertebrate fauna with dense calcite rims, 2BAk, PC1; (G) carbonate rhizoliths and high biogenic porosity, 3Bk, PC1.

Field magnetic susceptibility (FMS) was measured throughout the section every 3 cm using a portable kappameter PIMV. In the laboratory, soil colors were determined using the Munsell color chart for dry samples from each soil horizon (Munsell Color, 2000).

For grain-size analysis, samples were taken at vertical intervals of every 2 cm for the entire thickness of the section. Sample preparation included grinding the material, sequential removal of carbonates (using 10% HCl) and organic matter (using 30% H<sub>2</sub>O<sub>2</sub>), and peptization (using 4% Na<sub>4</sub>P<sub>2</sub>O<sub>7</sub>) (Varga et al., 2019). The grain sizes of all samples were measured using a Malvern Mastersizer 2000 laser diffraction particle-size analyzer in the Environmental Paleoarchives laboratory of the Institute of Geography of the Russian Academy of Sciences (Moscow). The sample was introduced into the HydroEV disperser unit and sonicated at 70% power for 100 seconds. Subsequently, seven repeated measurements were conducted after the ultrasonic unit was turned off, and the results were averaged using the Mastersizer v.3.62 Application. Particle size was calculated using the Mie theory, with refractive index values of  $n = 1.33$  for the dispersant,  $n = 1.55$  for the particles, and an absorption coefficient of  $k = 0.1$  (Özer et al., 2010). The following particle-size fractions were identified: clay  $\leq 2 \mu\text{m}$ ; fine silt  $> 2\text{--}6.3 \mu\text{m}$ ; medium silt  $> 6.3\text{--}20 \mu\text{m}$ ; coarse silt  $> 20\text{--}63 \mu\text{m}$ ; fine sand  $> 63\text{--}200 \mu\text{m}$ ; medium sand  $> 200\text{--}630 \mu\text{m}$ ; coarse sand  $> 630\text{--}2000 \mu\text{m}$ ; gravel  $> 2000 \mu\text{m}$ , according to the international scale ISO 14688-1:2017. Measurements of 40 randomly selected samples from each unit (L1, PC1, L2, PC2, L3) were used to construct grain-size distribution curves, showing the volume of particles (%) of a certain size ( $\mu\text{m}$ ). Base statistical parameters (arithmetic mean, median, mode, and skewness) for particle sizes were calculated. The U-ratio index (ratio between the 16–44  $\mu\text{m}$  and 5.5–16  $\mu\text{m}$  fractions), which reflects the strength of the wind during sedimentation (Vandenberghe et al., 1997) was calculated. The grain-size index (GSI; ratio between the 20–50 and  $< 20 \mu\text{m}$  fractions) was also calculated as an index of the cyclicity of wind intensity, as well as the combined influence of wind and precipitation regime (Rousseau et al., 2002).

Loose samples were taken from the middle part of each genetic paleosol horizon and separate morphologically distinct layers of PC1, L2, PC2, and L3 for analysis of chemical composition, as well as samples with an undisturbed structure for micromorphological studies. For the bulk chemical analysis, samples were sieved through a 1-mm sieve and measured for the content of macro- and microelements using energy-dispersive X-ray fluorescence methods in the Department of Chemistry and Physical Chemistry of Soils of the V.V. Dokuchaev Soil Science Institute. The contents of the elements are calculated for a non-calcined sample. The organic-carbon content was measured by Tyurin's method (Vorob'eva, 1998) without preliminary removal of carbonates. The method is based on the oxidation of soil organic matter with chromic acid to form carbon dioxide and back titration with ferrous ammonium sulfate. The analysis was carried out in the Laboratory of the Institute of Water Problems, Hydropower and Ecology NAST (Dushanbe).

Micromorphological properties were studied in thin sections of  $4 \times 5 \text{ cm}$  in size, made in the laboratory of mineralogy and micromorphology of soils of the V.V. Dokuchaev Soil Science Institute (patent 2728926). The description of thin sections was carried out according to international guidelines (Stoops, 2021) using an Olympus BX51 polarizing microscope with an Olympus DP26 digital camera. Soil processes were reconstructed based on neof ormation types in the paleosol horizons (Fig. 5).

## Results

### Stratigraphy and lithology

Generalized stratigraphic characteristics of the loess–paleosol series in the upper part of the Obi-Mazar are detailed in Supplementary Table 1. The entire sequence is affected by pedogenic processes to some extent. Boundaries between the layers and/or horizons are smooth and gradual. Paleosols and pedocomplexes are numbered from top to bottom. Horizons within each pedocomplex are numbered sequentially from top to bottom, such as 1ABk for the first soil and 2BAk for the second. Six units were identified from top to bottom in the stratigraphy of the upper part of the Obi-Mazar (Fig. 2B).

#### Unit 1 (HS) 0–0.38 m

Unit 1 (HS) is a Holocene soil classified as a Regosol (IUSS Working Group WRB, 2022) that is greatly eroded due to its location on a slope, active plowing in Soviet times, and its current use for grazing. The properties of the modern soil were not considered in this study.

#### Unit 2 (L1) 0.38–12.85 m

Unit 2 (L1) is calcareous loess with a characteristic vertical wall and weak pedogenic features. The loess consists of light yellowish brown (10 YR 6/4d; Munsell Color, 2000) structureless, silt loam texture, compacted aleurite with a small number of fine pores. There are five loess layers (L1.1–L1.5) with varying degrees of biological development in the structure of the unit.

#### Unit 3 (PC1) 12.85–16.1 m

Unit 3 (PC1) is a welded pedocomplex of light brown silt loam, weakly structured, that predominantly contains CaCO<sub>3</sub> concretions. Three paleosols (PC1.1, PC1.2, PC1.3) were distinguished in Unit 3 (PC1).

#### Unit 4 (L2) 16.1–18.68 m

Unit 4 (L2) is a calcareous pale-yellow loess, silt loam, slightly porous, structureless, with CaCO<sub>3</sub> concretions. Two layers (L2.1 and L2.2) are distinguished.

#### Unit 5 (PC2) 18.68–26.15 m

Unit 5 (PC2) is a compound polygenetic pedocomplex that is light brown to dark brown, from silt loam to silty clay loam, with CaCO<sub>3</sub> concretions and biolith capsules. Unit 5 contains two paleosols, PC2.1 and PC2.2, and two sublayers consisting of loess between them.

#### Unit 6 (L3) 26.15–34.86 m

Unit 6 is calcareous loess. Its main properties are similar to Unit 4 (L2). There are seven layers (L3.1–L3.7) distinguished by neof ormations.

The noted biolith capsules are chambers formed as a result of the vital activity of beetles of the family Tenebrionidae and subfamily Melolonthinae. They are found predominantly in Calcisols under an arid climate and form pupal chambers at depths of 0.3–1 m and in paleosols can record a period of relative stability of the land surface (Mestdagh et al., 1999). Their larvae for pupation form nests with a compacted calcareous wall. During burial, the capsules are filled with surrounding soil material (Valiakhmedov, 1977). Biolith capsules form round or ellipsoidal patterns in the layer. They are not lithified and consist of dense, compacted parent material having sometimes compacted carbonate rims (Dodonov and Lomov, 1985; Lomov and Ranov, 1985).



### Micromorphological properties

Micromorphological properties across all units show a porphyric distribution pattern (Stoops, 2021), predominantly featuring the silt fraction and rare scattered sand grains. Loess typically displays a massive microstructure with primary calcite grains. The groundmass is characterized by varying degrees of micritic impregnation and significant biogenic processing, along with a low content of amorphous organic-mineral clots. The latter are organic colloids associated with colloidal Si, Al, and/or Fe compounds. Rounded,

usually calcified excrements are found in the pores of all layers and horizons. The mineral compositions include quartz, feldspars, dark-colored minerals, including hematite, as well as micas and their weathered forms.

In layer L1.5, typical loess characteristics such as high porosity, abundance of silt material, and significant calcite impregnation are evident. Pedogenic features are minimal, including calcite redistribution (Fig. 3A), moderate content of organic-mineral clots near the pores, remains of rhizoliths, and signs of biological processing including excrements from invertebrate pedofauna and

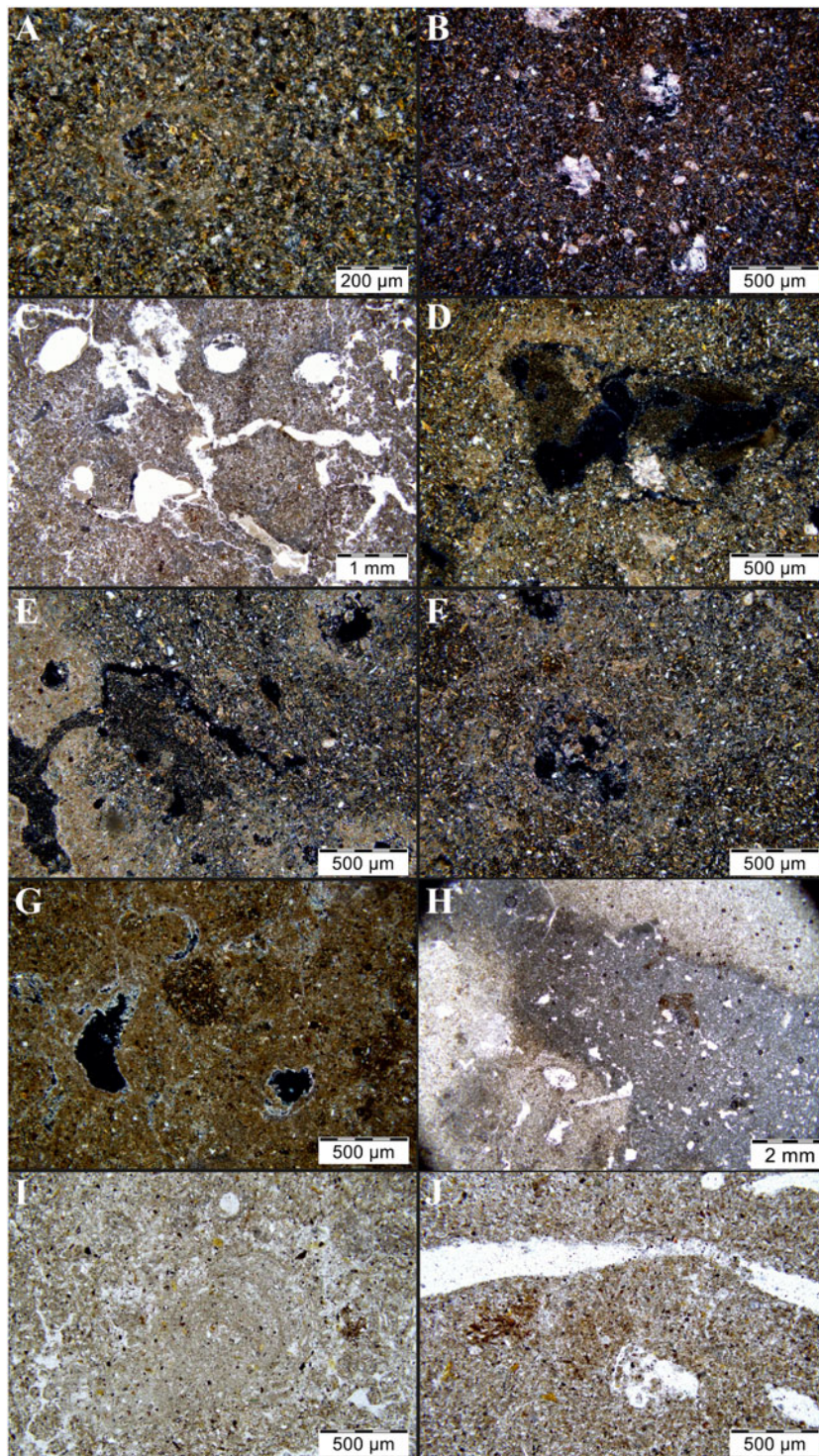


**Figure 3.** Microfeatures of the PC1 horizons, units L1 and L2 in the upper part of the Obi-Mazar section. XPL = cross-polarized light; PPL = plane-polarized light; GM = groundmass. (A) Calcite hypocoatings next to a pore with GM infill, L1.5, XPL; (B) clusters of calcite grains, 1ABk, XPL; (C) granular microstructure, silt coatings and infillings, and calcite coatings, 1BAk, PPL; (D) calcite grains, micritic-silt coatings and infillings, calcite hypocoatings, 2ABwk, XPL; (E) silt infillings, deep calcite hypocoatings, highly decalcified groundmass with speckled b-fabric, 2BAk, XPL; (F) calcareous excrement in pores and carbonate micronodules, 3ABk, XPL; (G) rounded humified aggregate inherited from a humus horizon, thin calcite coatings, 3Bk, XPL; (H) large porous calcite infilling with Fe-clots inside, 3BCwk, PPL; (I) silt crescent infilling, 3BCwk, PPL; (J) biogenic channels, micritic calcite coatings, organic-mineral clots, excrement, L2.2, PPL.

mollusk shell fragments. The groundmass here contains coarse calcite grains (Supplementary Table 1).

#### *Paleosol PC1.1*

Paleosol PC1.1 features horizons 1ABk–1BAk, with subtle pedogenic signs at the macroscopic level (Supplementary Table 1). At the microscopic level, pedogenesis is more evident. The 1ABk horizon is characterized by humus impregnation, a mostly granular coprogenic microstructure, and various coatings including calcite and Fe–Mn accumulations. The clusters of calcite grains are likely inherited from the loess (Fig. 3B). The underlying 1BAk horizon exhibits a channel microstructure with some granular microzones (Fig. 3C), few organic–mineral clots, and hypocoatings. Horizon 1BAk is extensively reworked by biota and includes clay–humus non-calcified aggregates. Unlike 1ABk, horizon 1BAk has stronger micritic impregnation, but lacks calcite grains and Fe–Mn hypocoatings and nodules.

#### *Paleosol PC1.2*

Paleosol PC1.2, comprising horizons 2ABwk–2Bkm–2BAk, exhibits more calcified residual zones, weakly calcified humus–clayey, multilayered calcite–humus–silty coatings (Fig. 3D) and infillings (Fig. 3E) than PC1.1. Paleosol PC1.2 shows an increased content of calcite grain clusters, with clay coatings noted in 2ABwk and multilayer coatings observed in 2BAk (silty coating over carbonate).

#### *Paleosol PC1.3*

With a profile of 3ABk–3Bk–3BCwk, Paleosol PC1.3 is saturated with small carbonate threads but lacks biolith capsules at the macroscopic level. It features acicular calcite (lubinite) coatings, with 3ABk showing humus impregnation and diverse calcite neoformations (e.g., coatings, hypocoatings, and nodules) (Fig. 3F). Horizons 3Bk and 3BCwk contain silty coatings, Fe–Mn nodules and hypocoatings, and non-calcified aggregates (Fig. 3G). Horizon 3BCwk has fragmentary clay coatings and silt-crescent infilling formed by earthworms or other invertebrates (Kooistra and Pulleman, 2018) (Fig. 3I). In addition, large infillings of highly calcified material with Fe nodules occur (Fig. 3H).

Layer L2.1 has clay–humus aggregates, like in the 3ABk horizon, and lots of excrement (Fig. 3J). Layer L2.2 is characterized by weak calcite impregnation. Clusters of calcite grains with destroyed boundaries and single-crystal gypsum leaching pores in the groundmass were observed.

#### *Paleosol PC2.1*

Paleosol PC2.1 has a profile 1BCk–1ABk–1ABwk–1Bwk–1Bkm–1Bk. Horizon 1BCk has a finer porous structure than L2. It contains rare calcite coatings, excrement, organic–mineral material (Fig. 4A), and gypsum leaching pores. Horizon 1ABk has a channel microstructure and non-calcified, weakly clayey groundmass with stipple-speckled and porostriated b-fabric. All pores have thin calcite coatings that grade into hypocoatings. Coatings of complex composition and structure (Fig. 4B) and many carbonate coatings consisting of calcified excrement and plant remains were observed. Horizon 1ABwk is characterized by an angular–blocky microstructure, significant humus content, clay, and dark-colored minerals. There are a large number of orthic aggregate Mn-hydroxide nodules and impregnated dendritic Fe–Mn-hydroxide nodules (Fig. 4C). Horizon 1ABwk also has clay–humus aggregates with diffuse (already assimilated) and sharp boundaries, a huge amount of calcified excrement, and sparite grains (Fig. 6). Horizon 1Bwk

has a dense near-pore micritic impregnation and a lots of calcite features. The gypsum-depleted pores form a loosened zone up to about 1 cm wide with characteristic edges for gypsum crystals (Fig. 4D). Horizon 1Bk is located under the calcic cemented horizon (carbonate crust) and has many infillings of calcareous excrement (Fig. 4E).

Loess (Ck) in PC2.1 separating the two paleosols shows evidence of high biogenic reworking and has many carbonate microfeatures. Calcite forms very thick hypocoatings and micritic and cytomorphic microsparite coatings. The gypsum-depleted pores (Fig. 4F) are twinned crystals and have the appearance of water intrusion. Currently, these pores have calcite hypocoatings. An increase in the content of dendritic Mn-organic nodules and hypocoatings predominantly associated with calcite hypocoatings was observed.

#### *Paleosol PC2.2*

Paleosol PC2.2 has a profile 2BAk–2BAwk–2Bkm–2Bk. Horizon 2BAk has calcite impregnation and various neoformations, shells (Fig. 4G), plant remains, humus zones, and hypocoatings. Horizon 2BAwk is a well-developed horizon because of dense reddish groundmass saturated with Fe and clay (Fig. 4H). The groundmass has an angular blocky structure and stipple-speckled b-fabric. Horizon 2Bk beneath the carbonate crust contains carbonized groundmass rich in clay and dark minerals, with extensive micritic hypocoatings (Fig. 4I) and larger calcite crystals.

Loess L3 is distinguished by high content of clay and dark-colored minerals. Microzonal calcite impregnation is noted, the pores have thick calcite hypocoatings and coatings. Layer L3.1 has signs of low biological activity including organic–mineral clots (Fig. 4J), destroyed excrement, and migration of carbonates. Mn-organic clots away from the pores are found in the groundmass. Layer L3.2 contains shells, organic–mineral hypocoatings, Mn-organic dendrites, single dense calcite micronodules, and clusters of calcite grains in the groundmass.

### *Grain-size composition*

The studied deposits in the Obi-Mazar section are characterized by a silty grain-size composition with high sorting indices (Fig. 8), which is why the compositional stratification within the section is poorly expressed. The sediments are dominated by the silt fraction ( $> 2\text{--}63\ \mu\text{m}$ ) making up over 87% of the material, while the clay fraction ( $\leq 2\ \mu\text{m}$ ) accounts for about 9.7% in the loess and 12% in the paleosols (Table 1). The highest clay fractions are found in PC1.2 and PC2.1, resulting in the lowest median and index values for these layers. The mean sand content generally remains under 1%, although localized peaks occur (Fig. 7).

The mean particle size in the studied sequence of the Obi-Mazar section is fairly uniform and fluctuates around  $15\ \mu\text{m}$  (Table 1), showing a maximum in units L1 and L2. The mean values for the layers decrease from loess to paleosols. The median particle-size ranges around  $11\text{--}12\ \mu\text{m}$  in loess and  $9\text{--}10\ \mu\text{m}$  in paleosols. The modal particle size ranges around  $17\ \mu\text{m}$  in loess and  $15\text{--}16\ \mu\text{m}$  in paleosols. The fractions have a monomodal distribution with a mode in the coarse dust fraction (Fig. 8). The particle distribution measured for each sample has positive skewness and positive-peaked kurtosis (i.e., a small spread in grain size). Throughout the entire thickness, the asymmetry remains virtually unchanged.

The U-ratio and GSI indices display almost identical curves, very similar in profile to other basic statistical parameters, with values typically below 0.97 and 0.37, respectively. Indices are



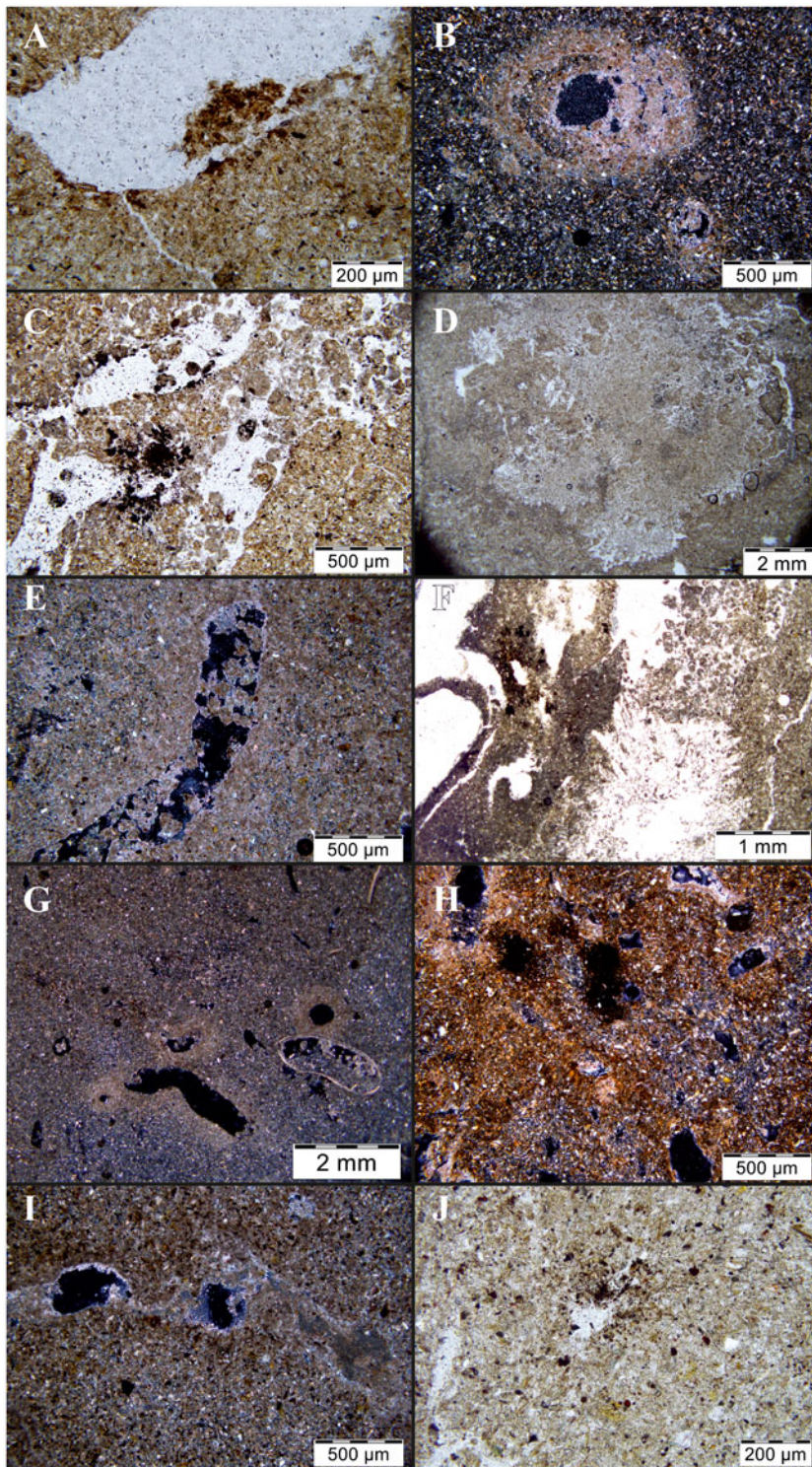


**Figure 4.** Microfeatures of the PC2 horizons and L3 in the upper part of the Obi-Mazar section. XPL = cross-polarized light; PPL = plane-polarized light, GM = groundmass. (A) Humus-mineral hypocoating and aggregate in a pore, 1Bck, PC2.1, PPL; (B) multilayer silt-calcite coatings with calcite hypocoating, 1ABk, PC2.1, XPL; (C) dendritic Mn-hydroxide nodule, carbonized excrement, 1ABwk, PC2.1, PPL; (D) gypsum leaching pores from water flow, 1Bwk, PPL; (E) intense calcite impregnation of GM, infilling of calcareous excrement covered by acicular calcite, 1Bk, XPL; (F) gypsum leaching pores, dendritic Mn-organic nodule, lots of excrement, Ck1 in PC2.1, PPL; (G) shells, calcite hypocoatings, 2BAk, XPL; (H) groundmass saturated by Fe and clay, orthic aggregate Mn-hydroxide nodule, 2BAwk, XPL; (I) silt infilling and excrement with micritic impregnation, 2Bk, XPL; (J) Mn-organic hypocoating, weathered mica, L3.1, PPL.

higher in loess layers, indicative of colder stages with strong winds, and lower in paleosols associated with weaker winds.

#### Chemical composition

The chemical composition of the LPS is relatively uniform. Statistical analysis showed no significant variation in  $\text{Na}_2\text{O}$  and  $\text{K}_2\text{O}$  content across soil horizons and loess layers (Fig. 9). However, in older Tajikistan LPS pedocomplexes, paleosols

often have lower Na and K levels than loess due to weathering and soil-forming processes, with Mg and Na being more actively removed than K (Yang et al., 2006).

The CaO content is higher in some soil horizons, likely due to strong carbonation, matching micromorphological evidence. The CaO levels are particularly high in horizons with abundant carbonate neoformations. The consistency of  $\text{SiO}_2$ ,  $\text{Al}_2\text{O}_3$ , and  $\text{Fe}_2\text{O}_3$  ratios across the LPS suggests a common loess source and minimal weathering of silicate minerals.

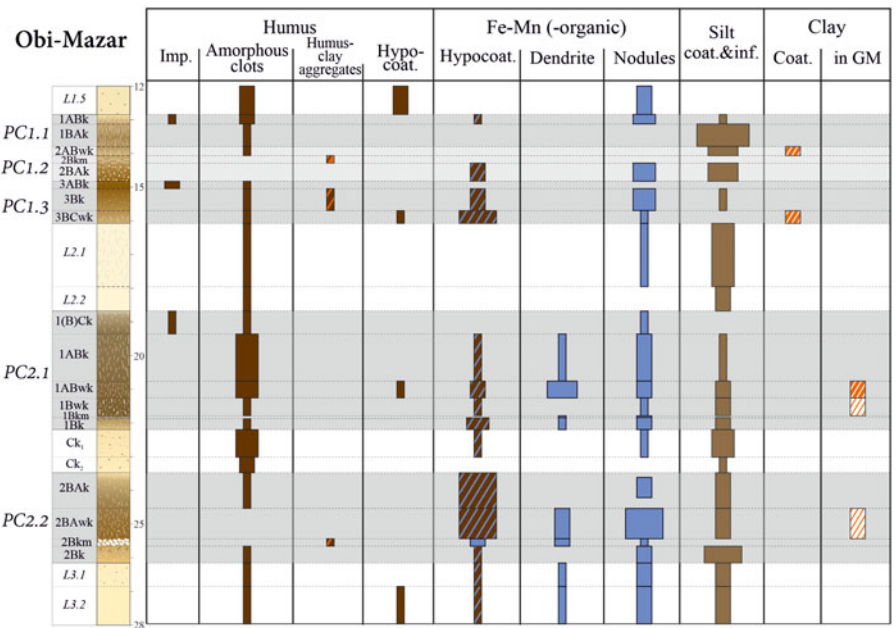


**Figure 5.** Degrees of occurrence of microfeatures in the studied paleosol horizons and loess layers of the Obi-Mazar section. The width of the column in the scheme reflects the frequency of occurrence of a genetic microfeature for each horizon. Imp. = impregnation; Coat. = coatings; Hypocoat. = hypocoatings; Inf. = infillings; GM = groundmass. Shaded areas indicate a mixture of two features.

Humus content is generally low, around 0.3%. In L1, organic matter varies between 0.06% and 0.70%, influenced by varying soil-formation intensities and climatic fluctuations, which affect the formation and preservation of organic matter. In the humus AB and BA horizons, humus content is higher, around 0.42%, but drops to 0.26% in the middle horizons. Humus levels in horizons PC1.3 (3Bk, 3BCwk) and L2 are approximately 0.14%.

## Discussion

### Correlation and chronology

Climatic variations in Central Asia, influenced by ice volumes in northern latitudes and solar insolation, are reflected in the Obi-Mazar section's LPS stratigraphy. Millennial humidity variability exhibits long, high amplitudes during interglacials and

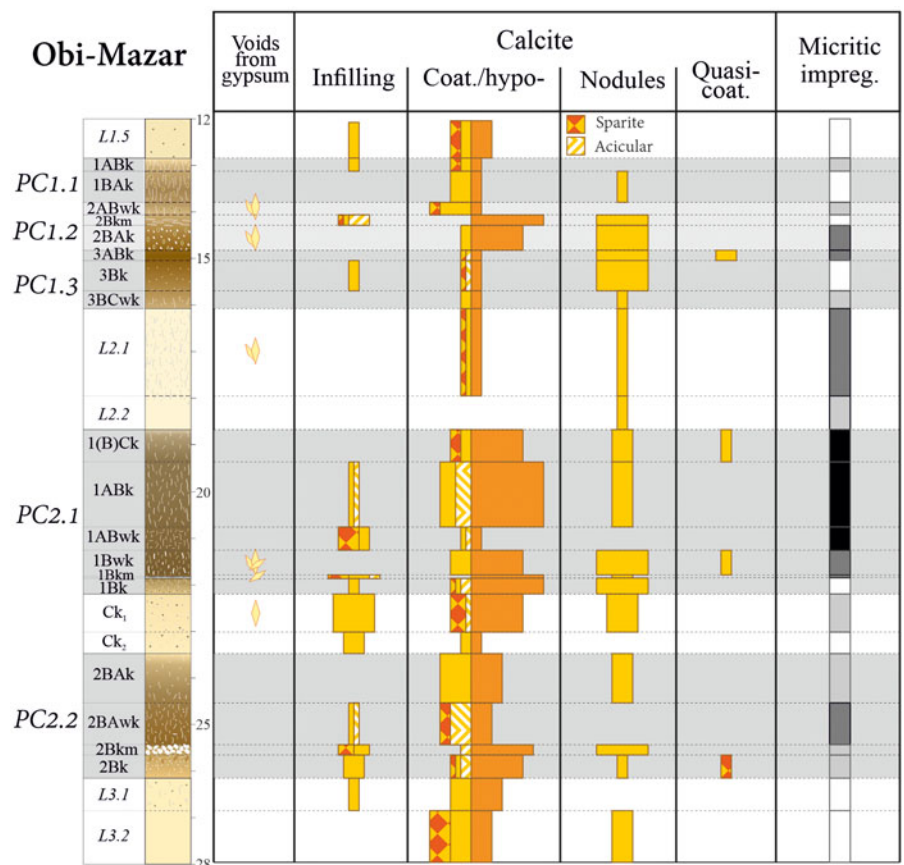


**Figure 6.** Degrees of occurrence of gypsum and calcite microfeatures in the studied paleosol horizons and loess layers of the Obi-Mazar section. The width of the column in the scheme reflects the frequency of occurrence of a genetic microfeature for each horizon. Impreg. = impregnation. Coat. = coatings; Hypocoat. = hypocoatings. In the column for micritic impregnation, 4 degrees of impregnation are distinguished: from white (crystallite), to black (the most leached).



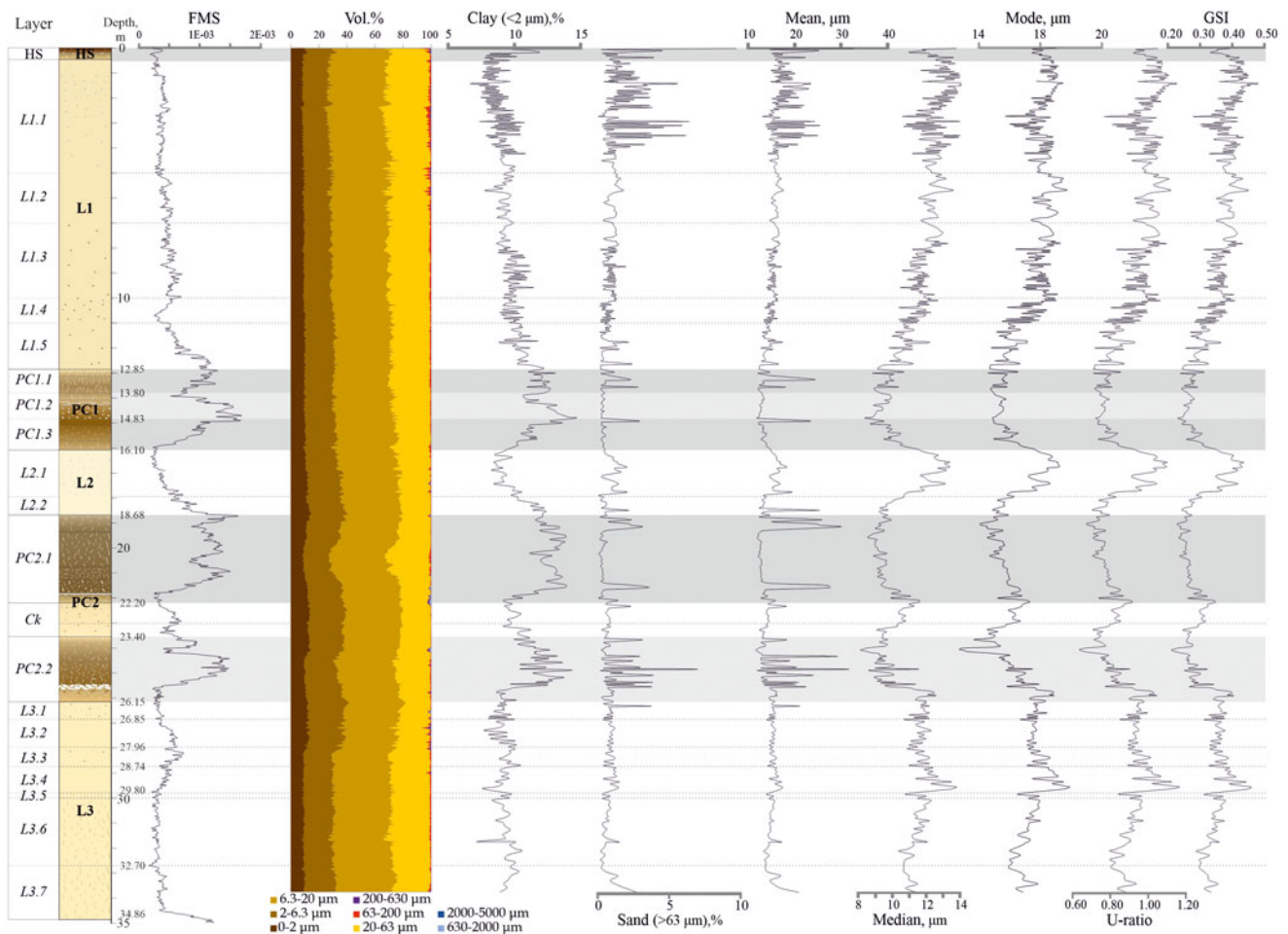


**Figure 7.** Stratigraphy and distribution of particle-size analysis data for the upper part of the Obi-Mazar section. FMS = field magnetic susceptibility.

short, low amplitudes during glacials, aligning with North Atlantic cooling rhythms (Fan et al., 2022). That is why the nature of the FMS curve of the Obi-Mazar section, as well as its stratigraphy and comparison with other LPS sections of Tajikistan, provide evidence for correlating the sediments of the Obi-Mazar section with the marine isotopic stages as orbital-scale records (Fig. 2) (Lisiecki and Raymo, 2005). Despite assumed hiatuses, the correlation with major glacial and interglacial cycles remains unaffected. The upper 35 m of the section, dating to the late and part of the middle Pleistocene, indicates a connection with the broader climatic context.

One of the debatable issues of the evolution of the LPS of the Khovaling Plateau is the problem of identifying the paleosols of stage MIS 3 (Alekseeva et al., 1977; Pospelova et al., 2005). Brief warming during MIS 3 led to the formation of 1–3 paleosols globally, such as the Bryansk soil in Eastern Europe and the Iskitim pedocomplex in Siberia (Volvakh et al., 2022) and the soil horizon in Northeast Asia (Velichko et al., 2017). In the Obi-Mazar section, layer L1.3 likely corresponds to MIS 3, which is suggested by a slight increase in FMS and annual precipitation (Song et al., 2014) and more stable U-ratio and GSI indices, indicating uniform wind strength and dustiness. Macroscopic-level evidence of soil processes in L1.3 and carbonate illuviation in L1.4 further support weak pedogenesis during this period. A thick layer corresponding to MIS 2 is also

distinguished in the Darai Kalon section (Dodonov et al., 2006), which has been dated to  $34.0 \pm 0.2$  ka (Frechen and Dodonov, 1998).

MIS 4, 3, and 2 are not distinguished either for Tajikistan or for the Tibetan Plateau, which is associated with the special influence of the Siberian anticyclone and the weakening of the Atlantic signal (Vandenberghe et al., 2006). In L1.5, the clear macro- and microfeatures of soil formation with increased FMS and content of the clay fraction may indicate a short and smooth transition between MIS 5 and MIS 4.

PC1, which is the first (uppermost) developed pedocomplex in the Afghan-Tajik depression, includes three paleosols. PC1 in the Obi-Mazar section does not have such a large thickness or loess layers between paleosols, unlike its counterpart in the Darai Kalon and Tagidjar sections (Mestdagh et al., 1999). There are two peaks on the FMS curve in PC1, however, PC1 contains three paleosols. MIS 5 probably was characterized by low loess accumulation, which suggests that formation of the upper paleosol (MIS 5a) affected not only the deposited loess but also the profile of the underlying paleosol (MIS 5c), partially welding paleosol profiles, akin to the Chinese Loess Plateau (Feng and Wang, 2006). The lower paleosol, which corresponds to MIS 5e, has a more differentiated profile and was less affected by later pedogenesis. The events that formed PC1 are similar to those described earlier (Mestdagh et al., 1999).

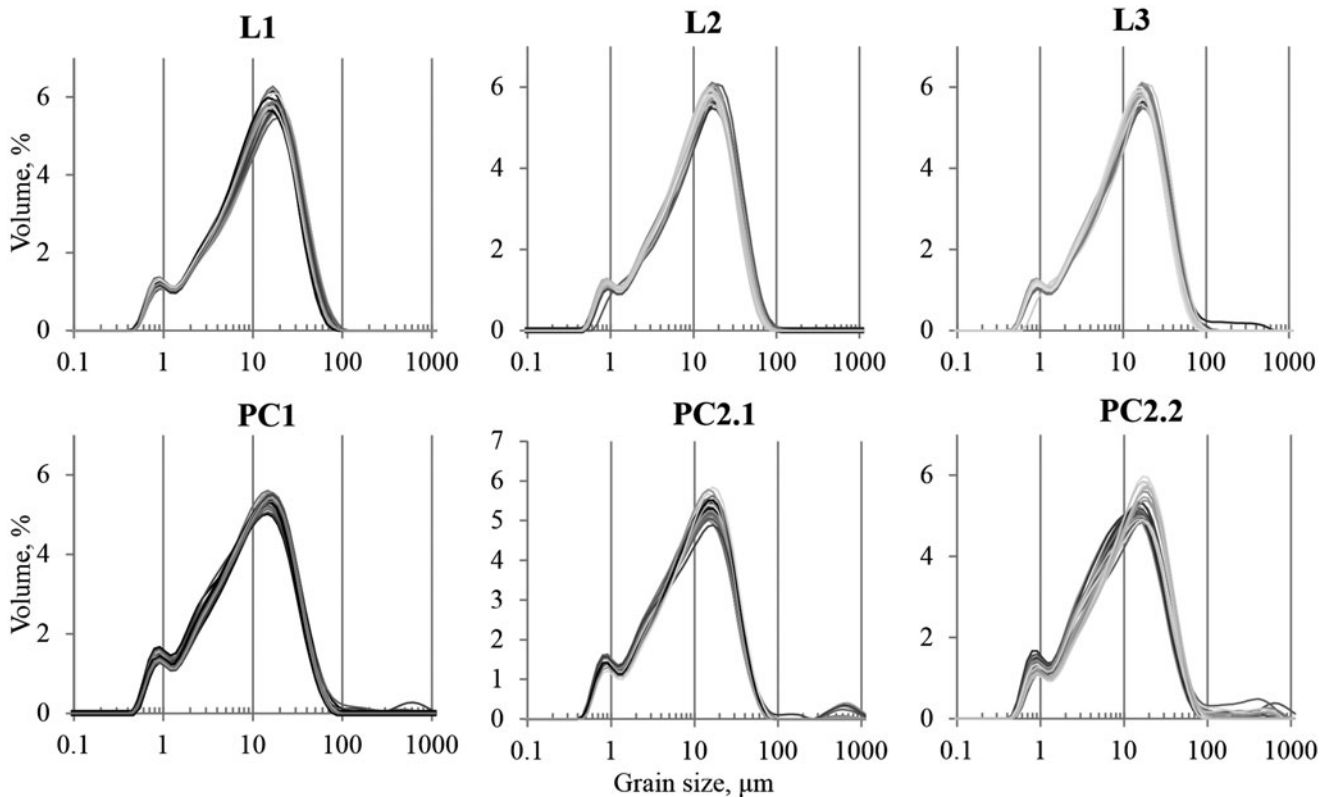


**Figure 8.** Grain-size distribution curves of studied PC1 and PC2 and loess units of the Obi-Mazar section.

Unit L2, which correlates with MIS 6, is noted for its low thickness and extensive pedogenic features. The FMS curve for the transition from L2 to PC1 is not uniform, which may indicate sediment erosion and that only the lower part of unit L2 is preserved (transition from MIS 7 to 6).

Unit PC2 consists of two paleosols. According to the grain-size composition and FMS, PC2.1 probably is a paleosol formed during MIS 7a–c, the underlying Ck formed during MIS 7d, and PC2.2 is a lower paleosol of MIS 7e. The increase in FMS and changes in U-ratio and GSI in L3 in the depth interval of 26.85–29.80 m (layers L3.2–L3.4) suggest a similar interstadial incipient paleosol formation as observed in L1.

### **Micromorphological features**

#### *B-fabric*

The b-fabric of the micromass is crystallitic for loess and weakly leached paleosol horizons (Fig. 6). Leaching of carbonates from groundmass occurs due to the action of large amounts of precipitation. In more-developed horizons such as ABwk, BAwk, and Bw (Fig. 4H) the b-fabric ranges from stipple-speckled to poro- and mono-striated, depending on the degree of clay mobility due to swelling and shrinking (Nettleton et al., 1969; Khormali and Kehl, 2011). Each paleosol except PC1.1 contains horizons with an index “w”.

#### *Calclitic pedofeatures*

Differentiating primary and secondary carbonates is crucial in understanding soil formation. While the nature of primary carbonates such as single crystals in the groundmass generally is clear, the genesis of secondary carbonates in the studied paleosols

remains questionable. They can be the result of recrystallization of calcite within the profile, or diagenetic features. It must be remembered that the same forms of carbonates can be formed under different conditions, including from recrystallization of calcite within a profile or diagenetic features (Kovda, 2008). Therefore, we present only the most-probable conditions of genesis in our opinion.

Primary (lithogenic) calcite grains and fragments of shells from terrestrial mollusks are frequent in loess. Coarse, welded calcite grains in the groundmass of L1 and upper horizons of PC1 paleosols (1ABk, 2ABwk) may be reworked by bioturbation (Kemp, 1995; Bronger et al., 1976), initially forming by calcite filling root parenchyma cells during long dry seasons (Becze-Deák et al., 1997). Grain clusters consist of several calcite crystals and vary between 50 μm and 150 μm, which exceeds the grain size of the coarse fraction. These grains often appear as microcodium (Retallack and Wright, 1990), which are radiating petal-shaped calcite crystals formed by symbiotic fungal-root activity (Klappa, 1991).

Sparite grains result from root-cell calcification during decarbonization of the groundmass, forming sparite calcite crystals, known as cytomorphic calcite, in the root channels (Jaillard, 1987; Durand et al., 2018). Their formation is linked to high rainfall and warm periods conducive to dense vegetation (Herrero et al., 1992).

Recrystallization of calcite and its migration up and down the profile are present in the form of coatings, hypocoatings, and nodules (Fig. 6). Carbonate coatings appear to be formed by dissolution and mechanical translocation (Siesser, 1973; Hay and Wiggins, 1991). Hypocoatings composed of micritic carbonate are formed from soil solutions percolating along the pores and



**Table 1.** Contents of fractions, statistical parameters and indices for stratigraphic layers of the Obi-Mazar section, calculated based on grain-size analysis. U-ratio index = ratio of fractions 16–44  $\mu\text{m}$ /5.5–16  $\mu\text{m}$ ; index GSI = ratio of fractions 20–50  $\mu\text{m}$ / $<20 \mu\text{m}$

| Layer     | Thickness [m] | Fraction content [%] |                |               |                |                | Characteristic particle diameter [ $\mu\text{m}$ ] |               |               |                 |                 | Distribution characteristics |  |  | Indices |  |
|-----------|---------------|----------------------|----------------|---------------|----------------|----------------|--|---------------|---------------|-----------------|-----------------|------------------------------|--|--|---------|--|
|           |               | Clay                 | Silt           | Sand          | Mean           | Median         | Moda   | Skewness      | Kurtosis      | U-ratio         | GSI             |                              |  |  |         |  |
| HS        | 0.38          | 9.8 $\pm$ 1.5        | 87.8 $\pm$ 3.5 | 2.4 $\pm$ 2.9 | 19.5 $\pm$ 5.8 | 12.2 $\pm$ 0.9 | 18.1 $\pm$ 0.6                                     | 1.4 $\pm$ 0.1 | 2.6 $\pm$ 0.3 | 1.01 $\pm$ 0.04 | 0.38 $\pm$ 0.03 |                              |  |  |         |  |
| L1        | 12.47         | 9.5 $\pm$ 0.9        | 89.4 $\pm$ 0.8 | 1.1 $\pm$ 0.9 | 16.1 $\pm$ 2.0 | 12.1 $\pm$ 1.0 | 17.8 $\pm$ 1.2                                     | 1.5 $\pm$ 0.1 | 2.7 $\pm$ 0.6 | 0.97 $\pm$ 0.09 | 0.37 $\pm$ 0.04 |                              |  |  |         |  |
| PC1.1     | 0.95          | 11.8 $\pm$ 0.7       | 87.4 $\pm$ 0.7 | 0.8 $\pm$ 0.7 | 14.5 $\pm$ 3.0 | 9.7 $\pm$ 0.5  | 15.1 $\pm$ 0.6                                     | 1.6 $\pm$ 0.1 | 3.1 $\pm$ 0.7 | 0.78 $\pm$ 0.04 | 0.27 $\pm$ 0.02 |                              |  |  |         |  |
| PC1.2     | 1.03          | 12.0 $\pm$ 1.3       | 87.2 $\pm$ 1.1 | 0.8 $\pm$ 0.8 | 13.9 $\pm$ 2.3 | 9.5 $\pm$ 0.5  | 15.1 $\pm$ 0.3                                     | 1.5 $\pm$ 0.1 | 2.7 $\pm$ 0.3 | 0.76 $\pm$ 0.02 | 0.26 $\pm$ 0.01 |                              |  |  |         |  |
| PC1.3     | 1.27          | 10.9 $\pm$ 1.3       | 88.6 $\pm$ 1.4 | 0.6 $\pm$ 0.5 | 14.1 $\pm$ 2.1 | 10.2 $\pm$ 1.0 | 15.9 $\pm$ 1.2                                     | 1.5 $\pm$ 0.1 | 2.5 $\pm$ 0.3 | 0.80 $\pm$ 0.05 | 0.28 $\pm$ 0.03 |                              |  |  |         |  |
| L2        | 2.58          | 9.5 $\pm$ 1.3        | 89.6 $\pm$ 1.2 | 0.9 $\pm$ 0.5 | 15.6 $\pm$ 2.1 | 11.6 $\pm$ 1.3 | 17.2 $\pm$ 1.5                                     | 1.5 $\pm$ 0.2 | 2.9 $\pm$ 1.1 | 0.92 $\pm$ 0.13 | 0.35 $\pm$ 0.07 |                              |  |  |         |  |
| PC2.1     | 3.52          | 11.8 $\pm$ 1.4       | 87.5 $\pm$ 1.7 | 0.7 $\pm$ 0.7 | 14.6 $\pm$ 3.9 | 9.7 $\pm$ 0.7  | 15.4 $\pm$ 0.8                                     | 1.7 $\pm$ 0.4 | 2.4 $\pm$ 0.3 | 0.77 $\pm$ 0.05 | 0.27 $\pm$ 0.03 |                              |  |  |         |  |
| PC2.1(Ck) | 1.2           | 9.8 $\pm$ 0.4        | 89.4 $\pm$ 0.4 | 0.7 $\pm$ 0.3 | 14.4 $\pm$ 0.9 | 10.5 $\pm$ 0.5 | 15.8 $\pm$ 0.7                                     | 1.5 $\pm$ 0.1 | 2.5 $\pm$ 0.4 | 0.82 $\pm$ 0.04 | 0.30 $\pm$ 0.02 |                              |  |  |         |  |
| PC2.2     | 2.75          | 11.2 $\pm$ 1.4       | 87.6 $\pm$ 1.8 | 1.2 $\pm$ 1.2 | 15.4 $\pm$ 4.1 | 9.9 $\pm$ 1.8  | 15.8 $\pm$ 1.8                                     | 1.6 $\pm$ 0.1 | 2.7 $\pm$ 0.4 | 0.82 $\pm$ 0.10 | 0.29 $\pm$ 0.05 |                              |  |  |         |  |
| L3        | 7.65          | 9.4 $\pm$ 0.8        | 89.8 $\pm$ 0.7 | 0.8 $\pm$ 0.5 | 15.1 $\pm$ 1.3 | 11.3 $\pm$ 0.9 | 17.1 $\pm$ 1.2                                     | 1.4 $\pm$ 0.1 | 2.8 $\pm$ 0.7 | 0.93 $\pm$ 0.07 | 0.36 $\pm$ 0.03 |                              |  |  |         |  |

penetrating the soil groundmass (Kemp, 1995). Acicular (needle-shaped) calcite formation in PC1.3 and PC2.1 is driven by fungal activity, with Mg predominating over Ca (Folk, 1974) and varies with seasonal contrasts (Becze-Deák et al., 1997; Bindschedler et al., 2012, 2016). Along with cytomorphic calcite, they indicate wetter and warmer conditions and denser plant cover (Khormali et al., 2006). Acicular calcite is the most mobile form of the carbonates present (Polyakov, 1989). Calcite coatings and hypocoatings may also result from diagenetic processes during loess accumulation in interglacials, with carbonates from airborne dust dissolving and settling in underlying layers when precipitation is below 750 mm/year (Schoeneberger et al., 2012).

The origin of pedogenic calcite nodules is influenced by a very large number of factors (Zamanian et al., 2016; Durand et al., 2018). It is likely that diffuse nodules of micritic calcite are formed due to weak impregnation of the groundmass. Leaching of impregnated micritic suggests rainfall exceeding 600 mm/year during soil formation (Yaalon, 1997; Schoeneberger et al., 2012). Layered calcite-silty coatings in the center of PC2 suggest a sequence of carbonate migration within the profile, followed by fine-grained silt movement and diagenetic calcite precipitation from leached loess dust. However, the question remains about the wetting front and the precipitation depth of calcite neoformations, the solution of which would help to reconstruct the paleoclimate.

Genesis of the calcite crust (Bkm horizon) is associated with the illuviation of calcite from the overlying horizons into the lower part of the most clayey Bw horizon (Schoeneberger et al., 2012).

#### Excrements and faunal galleries

Excrements or coprolitic aggregates observed in all loess layers and paleosol horizons are generally ellipsoidal or bacillo-cylindrical. Enchytraeid worms and oribatid mites produce these types of excrements (Bullock et al., 1985). They are associated with channels and round pores and have a variable calcareous composition (Mestdagh et al., 1999).

#### Gypsum pseudomorphs

Signs of the gypsum presence occur infrequently as rhombic and rosette-shaped voids (Fig. 6). Gypsum contents reach up to 0.1–0.2% (Lazarenko, 1977). Gypsum crystallized in the soil matrix at the boundary of the boundary of the groundmass and a solution saturated with gypsum, the result of which has the form of an intrusion. Subsequently, the leaching of gypsum occurred through the same intrusion pores, loosening the groundmass. This is different from the star-shaped gypsum joints in other PC1 layers (Mestdagh et al., 1999).

Gypsum is formed under arid to semiarid conditions with P/ET<sub>0</sub> (ratio of mean annual precipitation to mean annual reference crop evapotranspiration) < 0.4 or 300–400 mm annual rainfall (Khormali and Abtahi, 2003). Gypsum leaching indicates a change from arid conditions to more humid ones, under which a short-term leaching regime occurred. The formation and dissolution of gypsum in these paleosols are associated with the final stage of diagenesis since gypsum is more soluble than calcite and can crystallize more easily (Mestdagh et al., 1999). Gypsum leaching pores were observed in PC1.2, L2.1, and PC2.1 (1Bwk, Ck), indicating several very dry periods.

#### Clay coatings

The presence of clay coatings is quite rare (Fig. 5) and weakly expressed in only two horizons of PC1 (2ABwk, 2BCwk) without

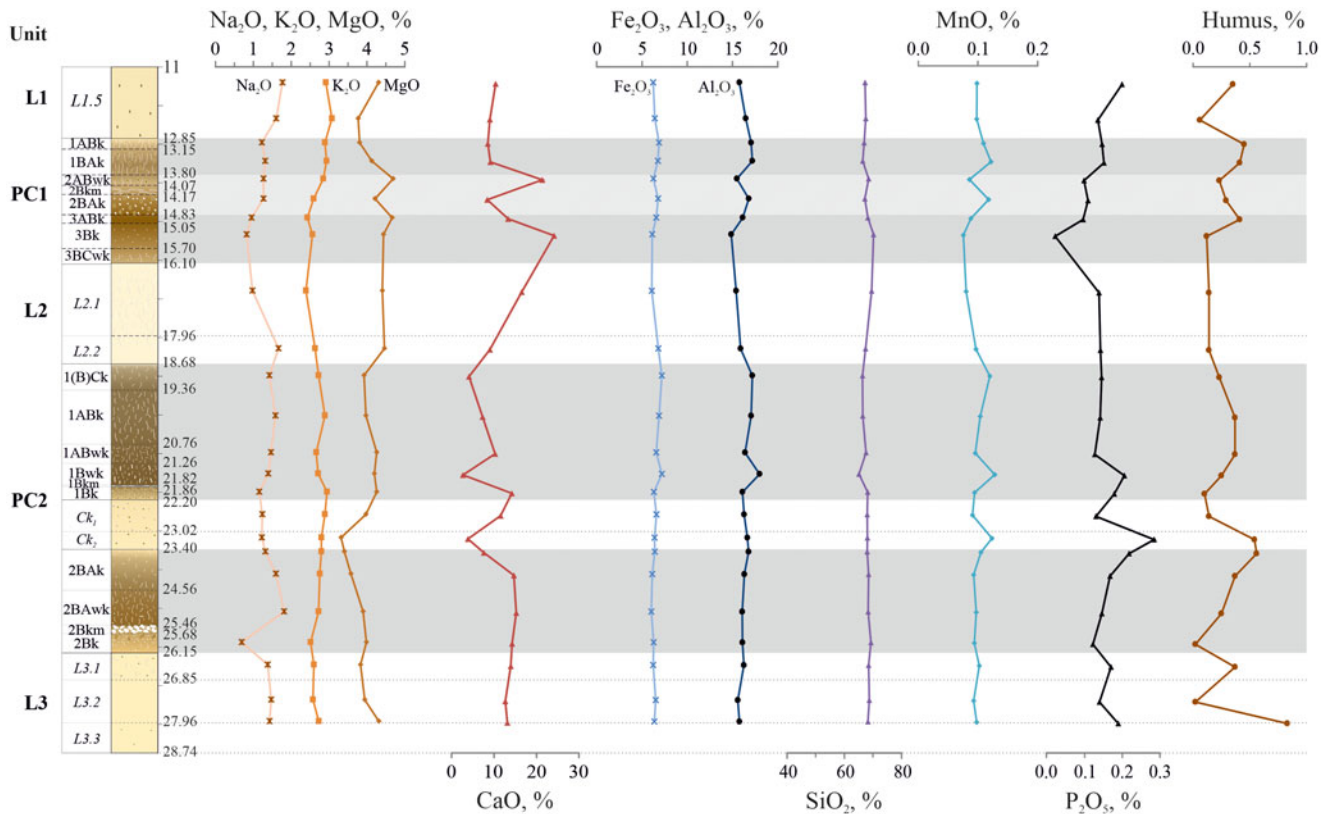


**Figure 9.** Distribution of chemical composition for the upper part of the Obi-Mazar section.

association with the illuvial process, which does not allow us to assign the index “t” to these horizons. Instead, these features, observed as mono- and porostriated clay orientations in the groundmass of PC2 (1ABwk–1Bwk, 2BAwk), result from in-situ weathering and indicate pedogenic changes rather than structural edge coatings (Bronger et al., 1998b), so we use the index “w” for these horizons. The movement of clays in calcareous soils occurs at the precipitation of about 800 mm/year when carbonates are leached and pH values are in the range of 5–7 (Scheffer and Schachtschabel, 2004; Khormali and Kehl, 2011). Partial decalcification and a pH decrease appear to be associated with temporary or short-seasonal moisture, which leads to local dispersion and intra-horizon mobility of clay particles with the formation of poorly developed Bw.

#### *Humus and organic-mineral complexes*

The humus content in the paleosols of Tajikistan is low since organic compounds are poorly preserved in arid conditions. Some upper horizons of PC1 and PC2 show residual humus impregnations and humus-clay, non-calcite aggregates with sharp boundaries, which potentially are remnants of eroded mollic horizons (Bronger et al., 1998a).

Organic-mineral complexes that include Fe and/or Mn are much more common (Fig. 5). Amorphous organic-mineral neoformations are represented by external nodules (clots) and hypo-coatings of Fe/Mn along organic residues. Factors influencing their genesis are described in detail in Vepřaskas et al. (2018). Hypocoatings were formed along small root channels, often influenced by intermittent water saturation and short, seasonal moisture that fosters transient waterlogging (Veneman et al., 1976; Hseu and Chen, 1999; Kyuma, 2004).

These neoformations generally accumulate in the lower parts of paleosol profiles, particularly above the Bkm crust in PC2.2 (Fig. 5), suggesting moisture saturation and stagnant water conditions above this dense horizon, which acted as an aquitard. The presence of amorphous nodules in subsoil loess layers is linked to downward diffusion of reduced Fe, where it is oxidized and precipitated as Fe-oxide neoformations (Stolt et al., 1994).

Overall, this description aligns with prior studies, although some variability might be due to microrelief effects (Bronger et al., 1998a, b; Mestdagh et al., 1999; Dodonov et al., 2006).

#### *Grain-size features*

The grain-size analysis of the Obi-Mazar section indicates that the LPS is homogeneous and well sorted, predominantly consisting of silt (> 2–63 μm) with minimal sand content, suggesting a rather distant location of the provenance (Yang et al., 2006) and stable sedimentation conditions with occasional interruptions and/or erosion (Ding and Ding, 2003).

The clay fraction peaks in PC1.2 and PC2.1, leading to lower median and index values in these layers, indicating the presence of Bw horizons (Table 1, Fig. 7). Unit PC2.1 shows two depth ranges with high clay content and corresponding peaks in FMS, hinting at overlapping paleosols during MIS 7a–c. The clay content in PC1 and PC2 of the Karamaidan and Darai Kalon sections is estimated at 20–35% (Dodonov et al., 2006; Bronger and Smolíková, 2019). Differences in measured clay content between this study and earlier works are due to varying methodologies. Classical sieve–pipette measurements overestimate clay content compared to more accurate laser diffractometry (Konert and Vandenberghe, 1997; Pabst et al., 2000; Yudina et al., 2020).



Sand content is generally higher in loess than in paleosols. However, PC2.2 shows unexplained low U-ratio and GSI values alongside a sharp increase in the sand fraction, which likely is due to short-term influence of nearby provenance such as river alluvium and covers of slope accumulations (Dodonov, 2002). Lower U-ratio indices for cold stages were also observed in the nearby Chashmanigar section (Ding et al., 2002). Layers L2.1 and L2.2 differ, which probably indicates strong differences in atmospheric circulation during the periods of their formation. Layer L2.1 shows characteristics of strong winds and high dust content in the atmosphere, while layer L2.2 matches the paleosol layers (Ding et al., 2002).

The studied LPS of the Obi-Mazar is similar to other Central Asian LPS with high silt content and increases in clay and fine-grained silt from loess to paleosols, indicating more intense soil formation and moisture during paleosol periods. However, Tajik LPS differ from others by the particle-size distribution processed by the end-member method. Observing the fine-grained edge of histograms, a characteristic asymmetry is noted, indicating the presence of an additional amount of silt in the 2–10  $\mu\text{m}$  range. One of the three end members has a modal grain size of 9  $\mu\text{m}$  in Tajik loess (Vandenberghe, 2013).

In the late Pleistocene loess of the Fergana Valley, the composition is predominantly silt at 88.3%, with sand at 2.8%, and clay at 8.9%. There is a notable increase in clay and decrease in sand with depth, especially in paleosols, where mean particle size can reach up to 33  $\mu\text{m}$  (Li et al., 2021). Tajik LPS have more clay, suggesting more humid conditions or different mineral compositions. Sand content varies more in Tajikistan, likely due to local relief and wind influence.

The Kyrgyz Tian Shan LPS, although similar to Tajik LPS, contains more sand and less clay. The content fractions average 12% sand, 80% silt, and 7% clay (Youn et al., 2014). Grain-size distribution in Tian Shan is more uniform than in Tajikistan, implying more stable sedimentation conditions.

Iranian loess, which is closer to its source, shows higher coarse-grained silt content compared to Tajik loess, indicating an increase in wind intensity during the Pleistocene (Vlaminck et al., 2016; Wang et al., 2017). The LPS of the Iranian Loess Plateau have higher U-ratio values and mean grain size, especially for loess layers. Upper Pleistocene LPS in both regions is systematically coarser than in Lower Pleistocene units, suggesting an increase of wind intensity during the Pleistocene. The upper Pleistocene LPS of Iran exhibits a trimodal grain-size distribution, whereas Tajik loess is mainly bimodal.

Tajik LPS, in terms of grain-size distribution, are similar to those of the Chinese Loess Plateau (Sun et al., 2002, 2004, 2006, 2010). The latter is characterized by a predominance of bimodal particle-size distributions with one mode in the fine-grained sand area and one in the fine-grained silt area. The mean grain size is 20–30  $\mu\text{m}$  (Vandenberghe, 2013; An, 2014), while the mean grain size for Tajik loess is 13–16  $\mu\text{m}$ . The grain-size distribution of the Chinese Loess Plateau allows for a good correlation with marine and ice-core records, whereas Tajik loess has specific changes in grain sizes making such correlation less clear (Vandenberghe et al., 2006). Tajik LPS demonstrate a higher frequency and amplitude of grain-size fluctuations compared to the loess on the Chinese Plateau, reflecting more dynamic climatic conditions in this region.

Chinese LPS resemble those of Tajikistan (Sun et al., 2002, 2004, 2006, 2010), mainly showing a bimodal particle-size distribution with modes in the fine-grained sand area and in the fine-grained silt area. The mean grain size is 20–30  $\mu\text{m}$

(Vandenberghe, 2013; An, 2014), while the mean grain size for Tajik loess is 13–16  $\mu\text{m}$ . While Chinese loess aligns well with marine and ice-core records by grain-size distribution, Tajik loess has distinct grain-size variations that make correlations less pronounced (Vandenberghe et al., 2006). The higher frequency and amplitude of grain-size fluctuations in Tajik loess indicate more dynamic climatic conditions in the region.

### Classification of studied paleosols

Despite the fact that it is quite difficult to classify paleosols according to modern classifications and not reasonable in all cases (Nettleton et al., 2000; Imbellone, 2011), we tried to correlate paleosols PC1 and PC2 according to the IUSS Working Group WRB (2022) in order to get some idea of the possible paleoenvironments.

Paleosol PC1.1 is a Haplic Calcisol. Nowadays, these soils are widespread and occupy steppes, hill slopes, and/or plateaus. The climate associated with these soils varies from Mediterranean to arid and semi-arid, with annual rainfall of 170–600 mm (Özden et al., 2001) and mean annual temperatures of 10–25°C. These soils have a wide distribution and occupy large areas in Turkey, Spain, North Africa, and the Middle East (Zdruli et al., 2011). The Khovaling Plateau soils were probably developed in semi-arid conditions under a xerophytic grassland (Mestdagh et al., 1999).

Paleosol PC1.2 is a Calcic Luvic Kastanozem. They are developed in semi-arid and sub-humid regions with 400–650 mm annual rainfall under Mediterranean sclerophyllous woodland and a short-grass steppe belt conditions. The soils are the most widespread in Europe (Dan et al., 1981; Badía-Villas and del Moral, 2016). The Khovaling Plateau vegetation was probably dominated by xerophytic grasses and shrubs in combination with some broad-leaf trees during the formation of this paleosol (Mestdagh et al., 1999).

A welded profile of PC1.1 and PC1.2 likely was promoted by low accumulation rates of aeolian dust over PC1.2. During PC1.1 formation, fine particles moved down the profile, settling as silt infillings in PC1.1 horizons, enriching horizon 2ABwk. Alternatively, the accumulation of fine-grained silt and clay in 2ABwk might be from carbonates being sequentially removed from the PC1.1 profile, forming horizontal carbonate interlayers in 2Bkm. The latter could represent an early stage of carbonate-crust formation, acting as a barrier to additional particle movement down the profile.

Paleosol PC1.3 is a Luvic Kastanozem. They often develop on loess parent materials and are associated with a dry and continental climate with relatively cold winters and hot summers. They are formed in regions where the average annual temperature is 8–9°C with 550–650 mm annual rainfall and a 0.75–0.9 P/ET<sub>o</sub> under subtropical oak–hornbeam forests and meadow ecosystems (Lomov et al., 1982; Lomov and Ranov, 1985; Tobiašová et al., 2013; Pospíšilová et al., 2020).

Both paleosols PC2.1 and PC2.2 are Luvic Petrocalcic Kastanozems. Kastanozems develop under a fairly wide range of conditions, but the averages are 15.5°C annual temperature, 1.16 P/ET<sub>o</sub>, and 550–650 or more mm annual rainfall (Costantini et al., 2013). They are formed from steppes to forests dominated by oak or hornbeam (after Spaargaren, 1994; Nestroy, 2001; Zdruli et al., 2011). The difference between PC2.1 and PC2.2 is that the latter forms in a relatively humid climate.

The results of Dodonov et al. (2006) and Mestdagh et al. (1999) are closest to this classification for the Tajik LPS, where

they distinguish the following taxa: PC1.1 – Haplic Calcisol or Serozem in the Russian classification (Egorov et al., 1987); PC1.2 – Luvi-Calcic Kastanozems (Carbonate Cinnamon soil); PC1.3 – Luvic Kastanozems (Leached Cinnamon soil); PC2.1 – Calcic Kastanozem (Carbonate Cinnamon soil); PC2.2 – Luvi-Endocalcic Kastanozems (Typical Cinnamon soil). In our opinion, the classification of Tajik paleosols as Phaezems is not entirely correct (Bronger et al., 1998a) because secondary carbonates are present in the paleosol profiles. This also applies to the Holocene soil, which does not yet have diagenetic signs, although the current amount of precipitation reaches 1000 mm/year (Yang and Ding, 2006). Moreover, Phaezems are not identified in the modern soil cover of Tajikistan (Khormali et al., 2024).

In the Chinese LPS, two paleosols are distinguished in the upper pedocomplex: MIS 5a–c paleosols, which can be correlated with Calcic Kastanozem or Luvic Phaeozem, and MIS 5e paleosols, which can be correlated with Luvic Kastanozem or a strongly rubificated Chromic Luvisol (Guo et al., 1993). Holocene soils are classified as Chernozem and Phaeozem. The late Pleistocene climate in this region was likely influenced by local agents and was wetter than in Tajikistan.

It is difficult to compare the studied paleosols with the Holocene ones since a complete, undisturbed profile of modern soil has not been described for this relief element and structure of soil cover. At this research stage, we can say that the paleosols of PC2 are closest to the modern soil in the area, but there are differences such as the presence of the Bkm horizon and biolith capsules in the paleosols.

## Conclusions

The studied 35-meter loess–paleosol sequence at the Obi-Mazar reference section on the Khovaling Loess Plateau, spanning the last 250 ka, probably formed under fairly stable conditions without significant breaks in sedimentation. The sequence consists of the first pedocomplex with three paleosols, correlated with MIS 5 (ca. 71–130 ka), and the second pedocomplex with two paleosols, correlated with MIS 7 (ca. 191–243 ka) of the regional chronostratigraphy of the Khovaling Loess Plateau.

Significant biological activity was noted in all loess layers and paleosol horizons. The distribution of calcite, Fe/Mn, and fine-grained silty and clayey neoformations reflect soil processes such as active humus formation, but rapid mineralization of organic matter, leaching of carbonates and gypsum, temporary soil moisture saturation, downward fine-grained particle movement, and weak clay weathering and mobility.

The deposits are characterized by a silty grain-size composition with high sorting indices leading to poorly expressed compositional stratification and indicating homogeneity in loess accumulation on the plateau. With about 90% silt, less than 1% sand, and 9–12% clay, the loess–paleosol series in Tajikistan differs from those in China and Iran. The chemical composition is fairly uniform, with a slight increase in humus in paleosol horizons. Structural, micromorphological, and grain-size characteristics, along with regional soil distribution, suggest the paleosols belong to the Calcisols–Kastanozems groups, with PC1 likely formed under drier conditions than PC2. Paleosol PC2 is closest to modern soil. Our results fit well into the context of previous studies of Tajik LPS.

**Supplementary material.** The supplementary data for this article can be found at <https://doi.org/10.1017/qua.2024.32>.

**Acknowledgements.** The work is supported by the Russian Science Foundation (Project №22-18-00568). P.M. Sosin, R.N. Kurbanov and I.K. Ashurmadov were supported by the NordForsk THOCA project (№105204). Prof. F. Khormali was supported by the Iran National Science Foundation under project 99006758.

## References

- Alekseeva, L.I., Bayguzina, L.L., Belsky, V.A., Vangengeim, E.A., Vislobokova, I.A., Gamov, L.N., Dmitrieva, E.L., et al., 1977. *Excursion guide: International Symposium on the Problem “Boundary of the Neogene and Quaternary System”*. Nauka, Moscow, 183 p. [in Russian]
- An, Z. (Ed.), 2014. *Late Cenozoic Climate Change in Asia: Loess, Monsoon and Monsoon-Arid Environment Evolution*. Springer, Dordrecht, The Netherlands.
- Badía-Villas, D., del Moral, F., 2016. Soils of the arid areas. In: Gallardo, J.F. (Ed.), *The Soils of Spain*. Springer, Cham, Switzerland, pp. 145–161.
- Becze-Deák, J., Langohr, R., Verrecchia, E.P., 1997. Small scale secondary CaCO<sub>3</sub> accumulations in selected sections of the European loess belt. Morphological forms and potential for paleoenvironmental reconstruction. *Geoderma* 76, 221–252.
- Bindschedler, S., Cailleau, G., Verrecchia, E., 2016. Role of fungi in the biomineralization of calcite. *Minerals* 6, 41. <https://doi.org/10.3390/min6020041>.
- Bindschedler, S., Milliere, L., Cailleau, G., Job, D., Verrecchia, E.P., 2012. An ultrastructural approach to analogies between fungal structures and needle fiber calcite. *Geomicrobiology Journal* 29, 301–313.
- Bronger, A., Bruhn-Lobin, N., Heinkele, T., 1993. Micromorphology of paleosols-genetic and paleoenvironmental deductions: case studies from central China, south India, NW Morocco and the Great Plains of the USA. In: Ringrose-Voase, A.J., Humphreys, G.S. (Eds.), *Soil Micromorphology: Studies in Management and Genesis*. Developments in Soil Science, Volume 22. Elsevier, Amsterdam, pp. 187–206.
- Bronger, A., Kalk, E., Schroeder, D., 1976. Über glimmer- und feldspatverwitterung sowie entstehung und umwandlung von tonmineralen in rezenten und fossilen Lössböden. *Geoderma* 16, 21–54.
- Bronger, A., Smolíková, L., 2019. Quaternary loess–paleosol sequences in East and Central Asia in comparison with Central Europe—micromorphological and paleoclimatological conclusions. *Boletín de la Sociedad Geológica Mexicana* 71, 65–92.
- Bronger, A., Winter, R., Derevjanko, O., Aldag, S., 1995. Loess–paleosol sequences in Tajikistan as a palaeoclimatic record of the Quaternary in Central Asia. *Quaternary Proceedings* 4, 69–81.
- Bronger, A., Winter, R., Heinkele, T., 1998a. Pleistocene climatic history of East and Central Asia based on paleopedological indicators in loess–paleosol sequences. *Catena* 34, 1–17.
- Bronger, A., Winter, R., Sedov, S., 1998b. Weathering and clay mineral formation in two Holocene soils and in buried paleosols in Tajikistan: towards a Quaternary paleoclimatic record in Central Asia. *Catena* 34, 19–34.
- Bullock, P., Fedoroff, N., Jongerius, A., Stoops, G., Tursina, T., 1985. *Handbook for Soil Thin Section Description*. Waine Research, Wolverhampton, UK, 152 pp.
- Costantini, E.A., Barbetti, R., Fantappiè, M., L’Abate, G., Lorenzetti, R., Magini, S., 2013. Pedodiversity. In: *The soils of Italy*. Springer, Dordrecht, Germany, pp. 105–178.
- Dan, J., Gerson, R., Koyumdjisky, H., Yaalon, D.H. (Eds.), 1981. *Aridic Soils of Israel: Properties, Genesis and Management*. Agricultural Research Organization, Institute of Soils and Water, Special Publication 190. Division of Scientific Publications, The Volcani Center, Bet Dagan, Israel, 190 pp.
- Ding, F., Ding, Z., 2003. Chemical weathering history of the southern Tajikistan loess and paleoclimate implications. *Science in China Series D: Earth Sciences* 46, 1012–1021.
- Ding, Z.L., Ranov, V., Yang, S.L., Finaev, A., Han, J.M., Wang, G.A., 2002. The loess record in southern Tajikistan and correlation with Chinese loess. *Earth and Planetary Science Letters* 200, 387–400.
- Dodonov, A.E., 2002. *Quaternary Period of Central Asia: Stratigraphy, Correlation, Paleogeography*. GEOS, Moscow, 254 pp. [in Russian]



- Dodonov, A.E., Baiguzina, L.L.**, 1995. Loess stratigraphy of Central Asia: palaeoclimatic and palaeoenvironmental aspects. *Quaternary Science Reviews* **14**, 707–720.
- Dodonov, A.E., Lomov, S.P.**, 1985. Stratigraphy and pedogenesis of loess formation of southern Tajikistan. In: Agrawal, D.P., Kusumgar, S., Krishnamurthy, R.V. (Eds.), *Proceedings of the Workshop on the Late Cenozoic Palaeoclimatic Changes in Kashmir and Central Asia, Ahmedabad, 19–23 October 1982*. Today & Tomorrow's Printers and Publishers, New Delhi, pp. 223–225.
- Dodonov, A.E., Pen'kov, A.V.**, 1977. Some data on the stratigraphy of the watershed loesses in the Tajik depression. *Bulletin of the Commission on the Quaternary Research* **47**, 67–76.
- Dodonov, A.E., Sadchikova, T.A., Sedov, S.N., Simakova, A.N., Zhou, L.P.**, 2006. Multidisciplinary approach for paleoenvironmental reconstruction in loess–paleosol studies of the Darai Kalon section, Southern Tajikistan. *Quaternary International* **152**, 48–58.
- Dodonov, A.E., Shackleton, N., Zhou, L.P., Lomov, S.P., Finaev, A.F.**, 1999. Loess–soil stratigraphy of the Quaternary of Central Asia: geochronology, correlation and evolution of the paleoenvironment. *Stratigraphy and Geological Correlation* **7**, 66–80. [in Russian]
- Durand, N., Monger, H.C., Canti, M.G., Verrecchia, E.P.**, 2018. Calcium carbonate features. In: Stoops, G., Marcelino, V., Mees, F. (Eds.), *Interpretation of Micromorphological Features of Soils and Regoliths*, second ed. Elsevier Science Bv, Amsterdam, Netherlands, pp. 205–258.
- Egorov, V.V., Fridland, V.M., Ivanova, E.N., Rozov, N.N., Nosin, V.A., Friev, T.A.** (Eds.), 1987. *Classification and Diagnostics of Soils of the USSR*. CRC Press, Boca Raton, Florida, 341 pp. [in Russian]
- Fan, Y., Jia, J., Liu, Y., Zhao, L., Liu, X., Gao, F., Xia, D.**, 2022. Millennial-scale climate oscillations over the last two climatic cycles revealed by a loess–paleosol sequence from central Asia. *Journal of Asian Earth Sciences* **240**, 105435. <https://doi.org/10.1016/j.jseae.2022.105435>.
- Feng, Z.D., Wang, H.B.**, 2006. Geographic variations in particle size distribution of the last interglacial pedocomplex S1 across the Chinese Loess Plateau: their chronological and pedogenic implications. *Catena* **65**, 315–328.
- Folk, R.L.**, 1974. The natural history of crystalline calcium carbonate; effect of magnesium content and salinity. *Journal of Sedimentary Research* **44**, 40–53.
- Frechen, M., Boergnik, W.**, 1997. Lobstratigraphie in Tadschikistan das Profil Darai Kalon. *Sonderveröffentlichungen des Geologischen Instituts der Universität zu Köln* **114**, 159–181.
- Frechen, M., Dodonov, A.E.**, 1998. Loess chronology of the middle and upper Pleistocene in Tajikistan. *Geologische Rundschau* **87**, 2–20.
- Gerasimov, I.P., Glazovskaya, M.A.**, 1960. *Fundamentals of Soil Science and Soil Geography*. State Department Geographical Literature, Moscow, 490 pp. [in Russian]
- Guo, Z., Fedoroff, N., Tung Sheng, L.**, 1993. Paleosols as evidence of difference of climates between Holocene and the Last Interglacial. *Quaternary Sciences* **13**, 41–55. [in Chinese with English abstract]
- Häggi, C., Eglinton, T.I., Zech, W., Sosin, P., Zech, R.**, 2019. A 250 ka leaf-wax  $\delta D$  record from a loess section in Darai Kalon, southern Tajikistan. *Quaternary Science Reviews* **208**, 118–128.
- Hay, R.L., Wiggins, B.**, 1991. Pellets, ooids, sepiolite and silica in three calcretes of the southwestern United States. In: Wright, V.P., Tucker, M.E. (Eds.), *Calcretes: An Introduction*. International Association of Sedimentologists Reprint Series 2, 51–68.
- Herrero, J., Porta, J., Fedoroff, N.**, 1992. Hypergypsic soil micromorphology and landscape relationships in Northeastern Spain. *Soil Science Society of America Journal* **56**, 1188–1194.
- Hseu, Z.Y., Chen, Z.S.**, 1999. Micromorphology of redoximorphic features of subtropical anthraquic Ultisols. *Food Science and Agricultural Chemistry* **1**, 194–202.
- Imbellone, P.A.**, 2011. Classification of paleosols. *Geociências* **30**, 5–13.
- IUSS Working Group WRB**, 2022. *World Reference Base for Soil Resources. International Soil Classification System for Naming Soils and Creating Legends for Soil Maps*. 4th edition. International Union of Soil Sciences (IUSS), Vienna, Austria. [https://www.isric.org/sites/default/files/WRB\\_fourth\\_edition\\_2022-12-18.pdf](https://www.isric.org/sites/default/files/WRB_fourth_edition_2022-12-18.pdf)
- Jaillard, B.**, 1987. Les structures rhizomorphes calcaires: modèle de réorganisation des minéraux du sol par les racines. D.Sc. dissertation, Université Montpellier 2, Montpellier, France. [in French]
- Kemp, R.A.**, 1995. Distribution and genesis of calcitic pedofeatures within a rapidly aggrading loess–paleosol sequence in China. *Geoderma* **65**, 303–316.
- Khormali, F., Abtahi, A.**, 2003. Origin and distribution of clay minerals in calcareous arid and semi-arid soils of Fars Province, southern Iran. *Clay Minerals* **38**, 511–527.
- Khormali, F., Abtahi, A., Stoops, G.**, 2006. Micromorphology of calcitic features in highly calcareous soils of Fars Province, southern Iran. *Geoderma* **132**, 31–46.
- Khormali, F., Kehl, M.**, 2011. Micromorphology and development of loess-derived surface and buried soils along a precipitation gradient in northern Iran. *Quaternary International* **234**, 109–123.
- Khormali, F., Valizadeh, S., Talebi, F., Tokareva, O., Schnider, R., Tazikeh, H., Sosin, P., Kurbanov, R., Buylaert, J.-P., Murray, A.**, 2024. Loess derived soils evolution in Tajikistan, implications for paleoclimate reconstruction. *3rd International IRQUA Conference on Quaternary Sciences* (January 29–February 1, 2024), Tehran, Iran, pp. 48–49.
- Khudzhageldiev, T.U.**, 2007. Stone industry from pedocomplex 6b of the Obimazar section (southern Tajikistan) according to excavations in 1997 y. *Archaeological work in Tajikistan, Academy of Sciences of the Republic of Tajikistan* **31**, 169–197. [in Russian]
- Klappa, C.F.**, 1991. Biolithogenesis of microcodium: elucidation. In: Wright, V.P., Tucker, M.E. (Eds.), *Calcretes: An Introduction*. International Association of Sedimentologists Reprint Series 2, 115–148.
- Konert, M., Vandenberghe, J.E.F.**, 1997. Comparison of laser grain size analysis with pipette and sieve analysis: a solution for the underestimation of the clay fraction. *Sedimentology* **44**, 523–535.
- Kooistra, M.J., Pulleman, M.M.**, 2018. Features related to faunal activity. In: Stoops, G., Marcelino, V., Mees, F. (Eds.), *Interpretation of Micromorphological Features of Soils and Regoliths*. Elsevier, Amsterdam, pp. 447–469.
- Kovda, I.V.**, 2008. Information value of carbonate formations for the reconstruction of processes and soil formation factors. In: Targulian V.O., Goryachkin S.V. (Eds.), *Soil Memory: Soil as a Memory of Biosphere–Geosphere–Anthroposphere Interactions*. LKI Publishers, Moscow, pp. 352–397. [in Russian]
- Kurbanov, R.N., Anoykin, A.A., Filimonova, T.G., Karaev, A.Ch., Meshcheryakova, O.A., Kulakova, E.P., Filatov, E.A., Chistyakov, P.V., Sharipov, A.F.**, 2022. Geoarchaeological research at the Honako III site in South Tajikistan in 2022. *Problems of Archeology, Ethnography, Anthropology of Siberia and Adjacent Territories* **28**, 157–163. [in Russian]
- Kyuma, K.**, 2004. *Paddy Soil Science*. Kyoto University Press and Trans Pacific Press, Melbourne, 280 pp.
- Lazarenko, A.A.**, 1977. Lithology of loess and buried soils. In: Dodonov, A.E., Melamed, Y.R., Nikiforova K.V. (Eds.), *International Symposium on the Neogene–Quaternary Boundary. Excursions Guide-book*. Scientific Editions, Moscow, pp. 122–124.
- Lazarenko, A.A., Pakhomov, M.M., Pen'kov, A.V., Shelkopyas, V.N., Giterman, R.E., Minina, E.A., Ranov, V.A.**, 1977. On the possibility of climatostratigraphic subdivision of the loess formation of Central Asia. *Pozdnie kainozoi Severnoi Evrazii (Late Cenozoic of Northern Eurasia)*. GIN AN SSSR, Moscow, pp. 70–133. [in Russian]
- Lisiecki, L.E., Raymo, M.E.**, 2005. A Pliocene–Pleistocene stack of 57 globally distributed benthic  $\delta^{18}O$  records. *Paleoceanography* **20**, PA1003. <https://doi.org/10.1029/2004PA001071>.
- Li, Y., Song, Y., Kaskaoutis, D.G., Zan, J., Orozbaev, R., Tan, L., Chen, X.**, 2021. Aeolian dust dynamics in the Fergana Valley, Central Asia, since ~30 ka inferred from loess deposits. *Geoscience Frontiers* **12**, 101180. <https://doi.org/10.1016/j.gsf.2021.101180>.
- Lomov, S.P.**, 1980. Fossil soils in forests and some features of their diagnosis in Tajikistan. In: Dodonov, A.E. (Ed.), *The Boundary of the Neogene and Quaternary System*. Moscow, pp. 98–102.
- Lomov, S.P., Ranov, V.A.**, 1985. The peculiarities of the Pleistocene palaeosol formations and distribution of embedded Palaeolithic tools. In: Agrawal, D.P., Kusumgar, S., Krishnamurthy, R.V. (Eds.), *Climate and Geology of Kashmir, the Last 4 Million Years : Proceedings of the International*

- Workshop on the Late Cenozoic Palaeoclimatic Changes in Kashmir and Central Asia, Ahmedabad, 19–23 October 1982.* Today & Tomorrow's Printers and Publishers, New Delhi, pp. 227–240.
- Lomov, S.P., Sosin, P.M.,** 1976. Soils of the Paleolithic camp site Karatau I in southern Tadjikistan. *Izvestiya Akademii Nauk Tajikskoy SSR*, pp. 93–99. [in Russian]
- Lomov, S.P., Sosin, P.S., Sosnovskaya, V.P.,** 1982. Structure and material composition of buried soils in Tajikistan. *Eurasian Soil Science* **1**, 18–30. [in Russian]
- Lomov, S.P., Tursina, T.V., Zhou, L.P.,** 1996. Magnetic susceptibility of soils: micromorphology and possible reconstructions of climate. *Soil Micromorphology. Studies in Soil Diversity, Diagnostics, Dynamics, 10th International Working Meeting on Soil Micromorphology (Moscow, Russia, July 8–13)*, p. 145.
- Mestdagh, H., Haesaerts, P., Dodonov, A., Hus, J.,** 1999. Pedosedimentary and climatic reconstruction of the last interglacial and early glacial loess–paleosol sequence in South Tadjikistan. *Catena* **35**, 197–218.
- Munsell Color,** 2000. *Munsell Soil Color Charts.* Munsell Color, Grand Rapids, MI.
- Nestroy, O.,** 2001. Classification of Chernozems, Phaeozems and Calcisols in Austria according to the World Reference Base for Soil Resources (WRB). *European Soil Bureau—Research Report* **7**, 121–124.
- Nettleton, W.D., Flach, K.W., Brasher, B.R.,** 1969. Argillic horizons without clay skins. *Soil Science Society of America Journal* **33**, 121–125.
- Nettleton, W.D., Olson, C.G., Wysocki, D.A.,** 2000. Paleosol classification: problems and solutions. *Catena* **41**, 61–92.
- Özden, M.O., Keskin, S., Dinç, U., Kapur, S., Akça, E., Şenol, S., Dinç, O.,** 2001. *Soil Geographical Database of Turkey at a Scale 1:1.000.000 4th Approximation.* Köy Hizmetleri Genel Müdürlüğü, APK Dairesi Başkanlığı, Ankara.
- Özer, M., Orhan, M., Işik, N.S.,** 2010. Effect of particle optical properties on size distribution of soils obtained by laser diffraction. *Environmental & Engineering Geoscience* **16**, 163–173.
- Pabst, W., Kuneš, K., Havrda, J., Gregorová, E.,** 2000. A note on particle size analyses of kaolins and clays. *Journal of the European Ceramic Society* **20**, 1429–1437.
- Pakhomov, M.M.,** 1991. Correlation of Pleistocene events in Central Asia and the dynamics of mountain zonality. *Izvestiya Akademii Nauk SSSR. Geographic Series* **6**, 94–103. [in Russian]
- Parviz, N., Shen, Z., Yunus, M., Zulqarnain, S.,** 2020. Loess deposits in southern Tajikistan (Central Asia): magnetic properties and paleoclimate. *Quaternary Geochronology* **60**, 101114. <https://doi.org/10.1016/j.quageo.2020.101114>.
- Polyakov, A.N.,** 1989. Micromorphological studies of calcite in chernozems of the European part of the USSR. *Soil Science* **2**, 79–86. [in Russian]
- Pospelova, G.A., Laukhin, S.A., Ranov, V.A., Vlasov, V.K., Volgina, V.A., Kulikov, O.A., Pilipenko, O.V., Sharonova, Z.V.,** 2005. New data on the chronostratigraphy of the upper regional buried soil of the loess section of Khonako-3, Tajikistan (archaeological, paleomagnetic and magnetic evidence). *Archaeology, Ethnography and Anthropology of Eurasia* **21**, 21–29(21), 21. [in Russian]
- Pospíšilová, L., Uhlík, P., Menšík, L., Hlisenkovský, L., Eichmeier, A., Horáková, E., Vlček, V.,** 2020. Clay mineralogical composition and chemical properties of Haplic Luvisol developed on loess in the protected landscape area Litovelské Pomoraví. *European Journal of Soil Science* **72**, 1128–1142.
- Railsback, L.B., Brook, G.A., Ellwood, B.B., Liang, F., Cheng, H., Edwards, R.L.,** 2015a. A record of wet glacial stages and dry interglacial stages over the last 560 kyr from a standing massive stalagmite in Carlsbad Cavern, New Mexico, USA. *Palaeogeography, Palaeoclimatology, Palaeoecology* **438**, 256–266.
- Railsback, L.B., Gibbard, P.L., Head, M.J., Voarintsoa, N.R.G., Toucanne, S.,** 2015b. An optimized scheme of lettered marine isotope substages for the last 1.0 million years, and the climatostratigraphic nature of isotope stages and substages. *Quaternary Science Reviews* **111**, 94–106.
- Ranov, V.,** 1995. The 'loessic Palaeolithic' in south Tadjikistan, central Asia: its industries, chronology and correlation. *Quaternary Science Reviews* **14**, 731–745.
- Ranov, V.A., Schäfer, J.,** 2000. Loess Paleolithic. *Archeology, Ethnography and Anthropology of Eurasia* **2**, 20–32. [in Russian]
- Retallack, G.J., Wright, V.P.,** 1990. Micromorphology of lithified paleosols. *Developments in Soil Science* **19**, 641–652.
- Rousseau, D.D., Antoine, P., Hatté, C., Lang, A., Zöller, L., Fontugne, M., Othman, D.B., et al.,** 2002. Abrupt millennial climatic changes from Nussloch (Germany) Upper Weichselian eolian records during the Last Glaciation. *Quaternary Science Reviews* **21**, 1577–1582.
- Schäfer, J., Ranov, V.A., Sosin, P.M.,** 1998. The “cultural evolution” of man and the chronostratigraphical background of changing environments in the loess palaeosol sequences of Obi-Mazar and Khonako (Tadjikistan). *Anthropologie* **36**, 121–135.
- Schäfer, J., Sosin, P.M.,** 2013. Am Fuße des Pamir—Archäologie in der Steilwand. *Archäologie in Deutschland* **2**, 12–16. [in German]
- Schäfer, J., Sosin, P.M., Ranov, V.A.,** 1996. Neue Untersuchungen zum Loesspaläolithikum am Obi-Mazar, Tádžikistán. *Archäologisches Korrespondenzblatt* **26**, 97–109. [in German]
- Scheffer, F., Schachtschabel, P.,** 2004. *Lehrbuch der Bodenkunde*, 13th Edition. F. Enke, Frankfurt, Germany. [in German]
- Schoeneberger, P.J., Wysocki, D.A., Benham, E.C. (Eds.),** 2012. *Field Book for Describing and Sampling Soils.* Government Printing Office, Washington, DC, 300 pp.
- Scientific and Applied Handbook on the Climate of the USSR,** 1988. Series 3. Long-term data. Part 1–6 (31). Tajik SSR, 398. [in Russian]
- Shackleton, N.J., An, Z., Dodonov, A.E., Gavin, G., Kukla, G.J., Ranov, V.A., Zhou, L.P.,** 1995. Accumulation rate of loess in Tajikistan and China: relationship with global ice volume cycles. *Quaternary Proceedings* **4**, 1–6.
- Siesser, W.G.,** 1973. Diagenetically formed ooids and intraclasts in South African calcretes. *Sedimentology* **20**, 539–551.
- Soil Survey Staff,** 2022. *Keys to Soil Taxonomy*, 13th edition. USDA Natural Resources Conservation Service. <https://www.nrcs.usda.gov/sites/default/files/2022-09/Keys-to-Soil-Taxonomy.pdf>.
- Song, Y., Hao, Q., Ge, J., Zhao, D., Zhang, Y., Li, Q., Zuo, X., Lü, Y., Wang, P.,** 2014. Quantitative relationships between magnetic enhancement of modern soils and climatic variables over the Chinese Loess Plateau. *Quaternary International* **334**, 119–131.
- Spaargaren, O.C. (Ed.),** 1994. *World Reference Base for Soil Resources. Draft.* Wageningen, Rome, 161 pp.
- Stolt, M.H., Ogg, C.M., Baker, J.C.,** 1994. Strongly contrasting redoximorphic patterns in Virginia Valley and Ridge paleosols. *Soil Science Society of America Journal* **58**, 477–484.
- Stoops, G.,** 2021. *Guidelines for Analysis and Description of Soil and Regolith Thin Sections.* John Wiley Sons, Hoboken, New Jersey.
- Sun, D., Bloemendal, J., Rea, D.K., An, Z., Vandenberghe, J., Lu, H., Su, R., Liu, T.,** 2004. Bimodal grain-size distribution of Chinese loess, and its palaeoclimatic implications. *Catena* **55**, 325–340.
- Sun, D., Bloemendal, J., Rea, D.K., Vandenberghe, J., Jiang, F., An, Z., Su, R.,** 2002. Grain-size distribution function of polymodal sediments in hydraulic and aeolian environments, and numerical partitioning of the sedimentary components. *Sedimentary Geology* **152**, 263–277.
- Sun, Y., An, Z., Clemens, S.C., Bloemendal, J., Vandenberghe, J.,** 2010. Seven million years of wind and precipitation variability on the Chinese Loess Plateau. *Earth and Planetary Science Letters* **297**, 525–535.
- Sun, Y., Lu, H., An, Z.,** 2006. Grain size of loess, palaeosol and red clay deposits on the Chinese Loess Plateau: significance for understanding pedogenic alteration and palaeomonsoon evolution. *Palaeogeography, Palaeoclimatology, Palaeoecology* **241**, 129–138.
- Tobiašová, E., Debska, B., Banach-Szott, M.,** 2013. Stability of organic matter of Haplic Chernozem and Haplic Luvisol of different ecosystems. *Journal of Central European Agriculture* **14**, 1541–1549.
- Valiakhmedov, V.,** 1977. Pupae chambers of soil-dwelling invertebrates in the gray soils of Tajikistan and their influence on the formation of the soil profile. *Eurasian Soil Science* **4**, 85–91. [in Russian]
- Vandenberghe, J.,** 2013. Grain size of fine-grained windblown sediment: a powerful proxy for process identification. *Earth-Science Reviews* **121**, 18–30.
- Vandenberghe, J., Renssen, H., van Huissteden, K., Nugteren, G., Konert, M., Lu, H., Dodonov, A., Buylaert, J.-P.,** 2006. Penetration of Atlantic



- westerly winds into Central and East Asia. *Quaternary Science Reviews* **25**, 2380–2389.
- Vandenbergh, J., Zhisheng, A., Nugteren, G., Huayu, L., Van Huissteden, K.**, 1997. New absolute time scale for the Quaternary climate in the Chinese loess region by grain-size analysis. *Geology* **25**, 35–38.
- Varga, G., Újvári, G., Kovács, J.**, 2019. Interpretation of sedimentary (sub) populations extracted from grain size distributions of Central European loess–paleosol series. *Quaternary International* **502**, 60–70.
- Veklich, M.F.**, 1979. Pleistocene loesses and fossil soils of the Ukraine. *Acta Geologica Scientiarum Hungaricae* **22**, 35–62.
- Velichko, A.A., Borisova, O.K., Zakharov, A.L.**, 2017. Change of landscape conditions in the south of the Russian Plain in the late Pleistocene based on the results of the study of the loess–soil series of the Sea of Azov. *Izvestiya Rossiiskoi Akademii Nauk. Geographic Series* **1**, 74–83. [in Russian]
- Veneman, P.L., Vepraskas, M.J., Bouma, J.**, 1976. The physical significance of soil mottling in a Wisconsin toposequence. *Geoderma* **15**, 103–118.
- Vepraskas M.J., Lindbo D.L., Stolt M.H.**, 2018. Redoximorphic features. In: Stoops, G., Marcelino, V., Mees, F. (Eds.), *Interpretation of Micromorphological Features of Soils and Regoliths*, 2nd Edition. Elsevier, Amsterdam, pp. 425–445.
- Vlaminck, S., Kehl, M., Lauer, T., Shahriari, A., Sharifi, J., Eckmeier, E., Lehdorff, E., Khormali, F., Frechen, M.**, 2016. Loess–soil sequence at Toshan (northern Iran): insights into late Pleistocene climate change. *Quaternary International* **399**, 122–135.
- Volvakh, A.O., Volvakh, N.E., Ovchinnikov, I.Y., Smolyaninova, L.G., Kurbanov, R.N.**, 2022. Loess–paleosol record of MIS 3–MIS 2 of north-east Cis–Salair plain, south of West Siberia. *Quaternary International* **620**, 58–74.
- Vorob'eva, L.A.**, 1998. *Chemical Analysis of Soils: Textbook*. Publishing House of Moscow State University, Moscow, 272 pp. [in Russian]
- Wang, X., Wei, H., Khormali, F., Taheri, M., Kehl, M., Frechen, M., Lauer, T., Chen, F.**, 2017. Grain-size distribution of Pleistocene loess deposits in northern Iran and its palaeoclimatic implications. *Quaternary International* **429**, 41–51.
- Yaalon, D.H.**, 1997. Soils in the Mediterranean region: what makes them different? *Catena* **28**, 157–169.
- Yang, S., Ding, F., Ding, Z.**, 2006. Pleistocene chemical weathering history of Asian arid and semi-arid regions recorded in loess deposits of China and Tajikistan. *Geochimica et Cosmochimica Acta* **70**, 1695–1709.
- Yang, S., Ding, Z.**, 2006. Winter–spring precipitation as the principal control on predominance of C<sub>3</sub> plants in Central Asia over the past 1.77 Myr: evidence from  $\delta^{13}\text{C}$  of loess organic matter in Tajikistan. *Palaeogeography, Palaeoclimatology, Palaeoecology* **235**, 330–339.
- Youn, J.H., Seong, Y.B., Choi, J.H., Abdrakhmatov, K., Ormukov, C.**, 2014. Loess deposits in the northern Kyrgyz Tien Shan: implications for the paleoclimate reconstruction during the Late Quaternary. *Catena* **117**, 81–93.
- Yudina, A.V., Fomin, D.S., Valdes-Korovkin, I.A., Churilin, N.A., Aleksandrova, M.S., Golovleva, Y.A., Philipov, N.V., Kovda, I.V., Dymov, A.A., Milanovskiy, E.Yu.**, 2020. The ways to develop soil textural classification for laser diffraction method. *Eurasian Soil Science* **53**, 1579–1595.
- Zamanian, K., Pustovoytov, K., Kuzyakov, Y.**, 2016. Pedogenic carbonates: forms and formation processes. *Earth-Science Reviews* **157**, 1–17.
- Zdruli, P., Kapur, S., Çelik, I.**, 2011. Soils of the Mediterranean region, their characteristics, management and sustainable use. In: Kapur, S., Eswaran, H., Blum, W.E.H. (Eds.), *Sustainable Land Management: Learning From the Past for the Future*. Springer, Berlin, pp. 125–142.